UiO : Department of Chemistry
University of Oslo

The Self-Diffusion Coefficient of Bulk Fluid Molecules Probed by Transverse Relaxation Measurements in an Inhomogeneous Magnetic Field

Master Thesis

Espen Hagen Blokkdal

June 2014

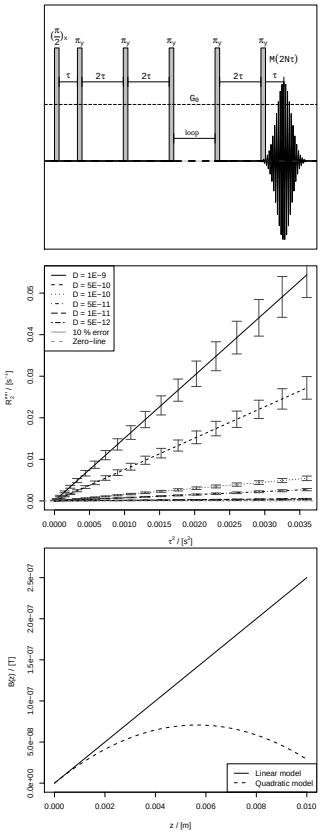

We shall not cease from exploration
And the end of all our exploring
Will be to arrive where we started
And know the place for the first time.

T. S. Elliot

Abstract

The possibility for performing self-diffusion measurements by Carr-Purcell-Meiboom-Gill (CPMG) experiments using the inherent magnetic field inhomogeneities as a gradient field were tested for six sample molecules, using a Maran Ultra NMR instrument with a 0.5 T permanent magnet. The method tested assumed that the magnetic field inhomogeneities could be approximated by a linear gradient, and the estimated parameter representing the magnetic field inhomogeneities in this model have been estimated to 25 μT^2 m^{-2}. The estimated diffusion coefficients were within 10-20 % of literature values, except for some samples, where convection was a problem The estimated field gradient have also been estimated from a Hahn echo experiment, and found to be consistent with the estimate from CPMG. The data obtained have also been used to probe the form of the magnetic field inhomogeneities, and have been found to be well described by a parabolic approximation. Some generalizations of the CPMG-signal was done to account for the parabolic form, which allows the CPMG-signal to be modified by introducing a correction function K, revealing the dependency of the sample height L, vertical displacement of the sample, ℓ, and the form of the NMR tube used.

Sensitivity analysis for the diffusion coefficient have been included, indicating that the diffusion coefficient may be detected as low as 10^{-11} m^2 s^{-1} at the instrument used. The sensitivity of the K-function for the various parameters have also been included, revealing the sample height as the most influential parameter.

The suitability for the free induction decay (FID) as an experiment for determining the transverse relaxation time have also been tested, and have been indicated to be unsuited for instruments with magnetic field inhomogeneities.

Preface

First of all, I would like to thank prof. Eddy W. Hansen for assigning me this project and for all the support, both with the experimental work and with the writing process. Without your help and encouragement, I would probably have given up by mid-September a year ago.

I would also like to thank PhD Candidate Marte S. M. Holmsen for all help with preparing my samples, and for the patience with me when I'm demonstrating why I didn't go into organic chemistry. Without your help, I would probably have destroyed a lot more equipment in the making of my samples.

A thank to Prof. Harald Walderhaug for his contribution to the writing process and telling me, time after time, that I must always communicate clearly, as it turns out that most of what I'm thinking stays inside my head until I have said it out loud. I would also thank you for spelling out to me that I'm allowed to use common sense when writing.

A special thanks to Anders L. Sundsdal for his help with preparing samples when Marte was busy with more important things, and for all the conversations during our not-to-frequent cycling. Without this I'd probably spent much more time pondering on strangely annoying things without progress.

Thank you, Bård, for two nice years of sharing office, and for all help with debugging code, solving problems and laughing. In my next life, I'll try to be at the office more of the time you spent there and less during the night. One day, when the night owls take over the world, I'll make sure you get to know what it feels like. That is, if I and the other night owls can be bothered to get out of bed in time.

Thank you very much, Jon, for helping me with Sobek when he decided to turn on me. Without your help, I would probably spent much more time screaming to a frozen screen than I think is sensible when writing together a thesis. And I would probably have written my thesis on a typewriter.

On a surprisingly clean note, I would like to thank Studentorchesteret Biørneblæs for contributing to conserving what is left of my sanity, although I trust we will debate the validity of that statement next March during the Christmas party.

On a personal note, I will end by thanking Lily for, in her very special own way and with her own means, making me remember that I can't sit in all night writing on my thesis. Without you, this thesis would have been finished a lot sooner and been totally unreadable.

Abbreviations and List of Symbols

Abbreviations

BTE Bloch-Torrey equation

CPMG Carr-Purcell-Meiboom-Gill

DMSO Dimethyl sulfoxide

FID Free Induction Decay

GNA Gauss-Newton algorithm

MRI Magnetic Resonance Imaging

NMR Nuclear Magnetic Resonance

`R` Open-source programming language. Specialized for statistical computing and data analysis

r.f. Radio frequency

THF Tetrahydrofuran

Mathematical symbols and notation

A, a A scalar
Written in italics

$\mathbf{A}, \mathbf{a}$ A vector
Written in boldface
Elements denoted A_i, a_i

$\mathbb{A}$ A matrix
Written as blackboard capitals
Elements denoted A_{ij}

$\langle A \rangle$ The ensemble average of A

δA The uncertainty in A

$\mathbf{i}, \mathbf{j}, \mathbf{k}$ The Cartesian unit vectors
The unit vector $\mathbf{k}$ will be taken to be parallel to $\mathbf{B}$

$\imath$ The irrational number
$\imath = \sqrt{-1}$

∇ The gradient operator
Written $\nabla = \mathbf{i}\frac{\partial}{\partial x} + \mathbf{j}\frac{\partial}{\partial y} + \mathbf{k}\frac{\partial}{\partial z}$ in Cartesian coordinates

∇^2 The Laplacian operator
Written $\nabla^2 = \frac{\partial^2}{\partial x^2} + \frac{\partial^2}{\partial y^2} + \frac{\partial^2}{\partial z^2}$ in Cartesian coordinates

Latin letters

$\mathbf{B}$ The magnetic flux density

c_i Concentration of component i

D Diffusion coefficient

$\mathscr{F}$ The Fourier transform

G_1 The magnetic field gradient

G_2 The magnetic field curvature

g The acceleration due to gravity
$g = 9.81$ m s^{-2}, [1]

Gr The Grashof number

J Scalar J-coupling constant

$\mathbf{J}$ Flux

k The ratio G_2/G_1

k_B The Boltzmann constant
$k_B = R/N_A = 1.38062259 \cdot 10^{-23} \pm 43 \cdot 10^{-26}$ J K^{-1}, [1]

L Sample height

ℓ Vertical displacement of NMR tube

$\hat{M}$ Normalized magnetization

$\mathbf{M}$ Magnetization vector

$\mathbf{m}$ Magnetic moment of a spin particle

N_A The Avogadro constant
$N_A = 6.02216940 \cdot 10^{23} \pm 6.6 \cdot 10^{20}$ mole^{-1}, [1]

$\bar{n}_i$ Number density of component i

P The propagator

Pr The Prandtl number

R The universal gas constant
$R = 8.3143435 \pm 42 \cdot 10^{-3}$ J mole^{-1} K^{-1}, [1]

r_0 The radius of the bottom hemisphere of a NMR tube

Ra The Rayleigh number

T Absolute temperature

Greek letters

α The coefficient of thermal expansion

γ The gyromagnetic ratio
$\gamma_{^1H} = 267.552 \cdot 10^6$ rad s^{-1} T^{-1}, [2]

Δ_∞ Limiting relaxation rate without the zero-correction R_2

$\delta(\mathbf{r})$ Dirac delta-function

Θ The characteristic temperature difference

κ Thermal diffusion coefficient

ν	Kinematic viscosity
ρ	The ratio r_0/L
ρ_i	Mass density of component i
τ	Inter-pulse time
ω	Resonance frequency

Relaxation-related symbols

T_1	Longitudinal relaxation time
R_1	Longitudinal relaxation rate $R_1 \equiv (T_1)^{-1}$
T_2	Transverse relaxation time
R_2	Transverse relaxation rate $R_2 \equiv (T_2)^{-1}$
T_2^*	Apparent T_2
R_2^*	Apparent R_2 $R_2^* \equiv (T_2^*)^{-1}$

Contents

List of Tables

List of Figures

Chapter 1

Introduction

1.1 Background

It is well known that Nuclear Magnetic Resonance (NMR) experiments such as the Hahn echo experiment, [3] and the Carr-Purcell-Meiboom-Gill (CPMG) experiment, [4, 5], may be used to probe self-diffusion in the presence of magnetic field gradients. Especially the CPMG-experiment has been applied to probe diffusion in various porous media where magnetic field inhomogeneities arise due to variations in the magnetic susceptibilities of the porous matrix, [6, 7].

Parallel to the work on characterizing how the magnetic field inhomogeneities in a porous media affects the NMR signal is the generalizations of the various model equations to account for magnetic field inhomogeneities and diffusion. The first major work was the improvement of the Bloch-equation, [8], by Torrey to include diffusion, [9]. The original papers of Hahn, Carr, Purcell, Meiboom and Gill assumed a linear gradient in the magnetic field. However, generalizations to account for more general models such as the parabolic magnetic field have been made, [10].

There are a number of reasons to perform self-diffusion measurements, which range from applications in the petroleum industry, [7], paint development, [11, 12], for the development of conservation techniques in archeology, [13], and identifying fruit juice, [14]. In medicine, diffusion measurements using Magnetic Resonance Imaging (MRI) are used in order to examine how water moves in tissue, allowing for a non-invasive examination, [15]. In addition, self-diffusion is an important factor in chemical engineering as it may be the rate-limiting factor for a given process, [16]. Therefore, self-diffusion measurements are relevant for actors in chemistry, medicine, and engineering.

The conventional technique for performing diffusion measurements is Pulsed Field Gradient (PFG) NMR, [17]. The principle of PFG is the application of

a gradient in the magnetic field across the sample by use of a gradient coil. The spatial variation of the local magnetic fields acts as a way of "labeling" the molecules, which in turn allows for estimating the diffusion coefficient and other properties related to translational motion.

Diffusion measurements by PFG does have some advantages over CPMG. The most immediate is the fact that PFG-techniques are established, and have been used for a wide variety of purposes with great success, [17, 18].

During this research project, some limitations regarding which systems that might be probed by CPMG for diffusion measurements were noted. These limitations will be commented on in chapter 5.

1.2 Motivation

The main goal of this project has been to examine the possibility for determining the self-diffusion coefficient of bulk fluids using CPMG experiments only, without implementing the gradient coils that provides the magnetic field gradients. It is these coils that is the typical "diffusion hardware". Other goals have been to

- Investigate the practical/experimental limitations and advantages of using CPMG-experiments to measure self-diffusion
- Derive models accounting for the effects of an inhomogeneous magnetic field on the various experiments used
- Derive model equations for extracting the diffusion coefficient D
- To identify the parameters (sample height, shape of sample tube and sample position in the magnetic field) and their significance on the NMR signal

By now, it should be clear why the self-diffusion measurements are done and why various actors are interested in making diffusion measurements. As pr. 30.04.2014, the price for a NMR instrument similar to the one in this work, set up to do conventional diffusion measurements by PFG-NMR is quoted by Anvendt Teknologi as 750 000 NOK*, whereas the same equipment without these components is quoted as 500 000 NOK. As the "diffusion hardware" adds another 50 % to the instrumental cost it is of interest to know that simple diffusion measurements may be performed by simple CPMG experiments without the need for these components.

*Pr. 30.04.2014, 1 NOK = 0.120805 €=0.167455 $ = 0.0993140 £

1.3 Outline of Thesis

Chapter 2 reviews the relevant theory of diffusion and NMR. This chapter also contains some generalizations of the free induction decay (FID), Hahn echo and CPMG signal as they are highly relevant to the discussion of the results.

Chapter 3 reviews the experiments used for obtaining the data sets together with how they were treated numerically. The various pulse sequences are presented in this chapter.

Chapter 4 reviews the experimental information about the samples and experimental settings used. A modification of the experiments for systems with long longitudinal relaxation times is also presented here.

Chapter 5 presents the results obtained and the discussion of these. All relevant parameters that can be estimated from the raw data are presented here, such as relaxation times and diffusion coefficients.

Chapter 6 presents the conclusions that can be drawn from the derived equations and experimental results.

Appendix A presents an algorithm for producing a list of time values that ensures evenly spacing of the recorded intensities when performing an inversion recovery-experiment together with an implementation as an `R` -script. This was used when performing inversion recovery-experiments in order to estimate the longitudinal relaxation time T_1 for the various systems used.

Appendix B presents the worked results of a steady-state magnetization when dealing with systems with long T_1. These results have been used to perform some of the measurements, as it allows for faster experiments. The appendix also includes simulations showing how fast such a steady-state magnetization is established.

Appendix C includes the scripts written for analyzing the CPMG-data and producing the CPMG-curves.

Appendix D shows how a second-order magnetic field inhomogeneity affects the CPMG- and Hahn echo responses within a cylindrical sample. This gives the basic idea on how to derive the expression presented by the end of chapter 2 and in [19].

1.3.1 The B-field vs. the H-field

In several of the references given in this thesis, the original equations were expressed in terms of the **H**-field, the magnetic intensity given in SI-units of Ampere pr. meter, whereas they are here expressed in terms of the **B**-field, the magnetic flux density given in SI-units of Tesla. In most materials, these

are proportional and in the same direction with the proportionality constant being the magnetic permeability, [20].

Chapter 2

Theory

The scope of this chapter is to give an introduction to the general theory and the equations used to design experiments and treat the obtained data.

2.1 Concepts of Diffusion

One of the most fundamental transport processes of any solution is diffusion.

There are two forms of diffusion: one is the flux due to gradients in any form of potential, such as chemical potential, free enthalpy, free energy etc. This will hereafter be referred to as gradient-driven diffusion or macroscopic diffusion. The other form is due to molecular collisions, resulting in random motion. This will hereafter be referred to as self-diffusion.

2.1.1 Gradient-Driven Diffusion

The first work on gradient-driven diffusion was on inhomogeneous mixtures studied from a macroscopic point of view. The results of this work can be formulated as Fick's first law of diffusion, [21];

$$\mathbf{J} = -\mathbb{D} \cdot \nabla \bar{n} \tag{2.1}$$

with $\mathbf{J}$ being the flux, $\bar{n} = \partial n / \partial V$ being the number density, ∇ the gradient operator and the self-diffusion tensor $\mathbb{D}$, giving the general expression for the flux of the components in a N-nary mixture. The diffusion tensor $\mathbb{D}$ can usually be replaced by a diffusion coefficient D as macroscopic techniques can not easily distinguish between the different modes of diffusion. In the case of self-diffusion, the diffusion tensor is replaced by a self-diffusion coefficient. In either case, the above equation then simplifies to

$$\mathbf{J} = -D \nabla \bar{n} \tag{2.2}$$

2.1.2 Self-diffusion

When there is no macroscopic diffusion, it becomes possible to observe self-diffusion in a system. Self-diffusion, also known as Brownian motion or random walk, is the random motion of particles that stems from the properties of matter; matter consists of atoms that never stand still, and this constant motion leads to collisions that is observable on a microscopic scale, [22]. In order for the self-diffusion not to be obscured by gradient-driven diffusion, it is necessary to minimize any gradients, as even relatively small gradients will induce a flux several orders of magnitude larger than the self-diffusion.

The law that governs self-diffusion is easily derived by assuming incompressibility of the liquid, that is;

$$\nabla \cdot \mathbf{v} = 0 \tag{2.3}$$

with $\mathbf{v}$ being the velocity field of the liquid. This follows when the number density $\bar{n}$ is assumed to be constant, which is equivalent to assuming conservation of mass and that no chemical reactions take place. From fluid mechanics, conservation of mass may be expressed as, [23];

$$\frac{\partial \bar{n}}{\partial t} = -\nabla \cdot (\bar{n}\mathbf{v}) = -\bar{n}\nabla \cdot \mathbf{v} - \mathbf{v} \cdot \nabla \bar{n} = -\nabla \cdot \mathbf{J} \tag{2.4}$$

and by substituting eq. 2.4 into eq. 2.2, with the use of eq. 2.3, the obtained equation is

$$\frac{\partial \bar{n}(\mathbf{r}, t)}{\partial t} = D\nabla^2 \bar{n}(\mathbf{r}, t) \tag{2.5}$$

where ∇^2 is the Laplacian operator. Equation 2.5 is referred to as the self-diffusion equation, and the solutions with appropriate boundary conditions yields the corresponding forms of the diffusion. Equation 2.5 might be expressed in terms of mass density ρ or concentration c by proper substitution.

If the solution of the self-diffusion equation is taken as a probability of a particle moving in a certain direction, the number density $\bar{n}$ might be substituted with the propagator, P, which is dimensionless. This transform might be seen as simply scaling the equation by $P = \frac{\bar{n}}{\bar{n}_0}$ with $\bar{n}_0$ being a suitable scaling of number density. This gives:

$$\frac{\partial P(\mathbf{r}, t)}{\partial t} = D\nabla^2 P(\mathbf{r}, t) \tag{2.6}$$

with the solution of eq. 2.6 dependent on the imposed boundary conditions. The most simple solution, useful for illustrating the nature of self-diffusion, is that of free, isotropic diffusion with the initial condition of a particle at origin. The initial condition is then represented by the Dirac delta-function,

$P(0,0) = \delta(r)$ and the boundary condition as $P(r \to \infty, 0) \to 0$. Under these assumptions, the Laplacian might be rewritten as

$$\nabla^2 \to \partial^2/\partial\xi^2$$

with ξ as the distance the particle travels from the origin, replacing $\mathbf{r}$. Equation 2.7 then reads

$$\frac{\partial P}{\partial t} = D\frac{\partial^2 P}{\partial \xi^2} \tag{2.7}$$

The solution might be obtained by Fourier transform. The general form of the Fourier transform will be taken as, [24];

$$\tilde{f}(\omega) = \mathscr{F}\{f(t)\} = \frac{1}{\sqrt{2\pi}}\int_{-\infty}^{\infty} f(t)e^{-\imath\omega t}\mathrm{d}t$$

with the inverse transform given as

$$f(t) = \mathscr{F}^{-1}\left\{\tilde{f}(\omega)\right\} = \frac{1}{\sqrt{2\pi}}\int_{-\infty}^{\infty} \tilde{f}(\omega)e^{\imath\omega t}\mathrm{d}\omega$$

when the kernel of the Fourier transform is taken to be $e^{-\imath\omega t}$.

When the Fourier transform is applied to eq. 2.7 with kernel $e^{-\imath k\xi}$, the equation transforms as:

$$\mathscr{F}\left\{\frac{\partial P(\xi,t)}{\partial t}\right\} = \frac{\mathrm{d}\tilde{P}(k,t)}{\mathrm{d}t} = \mathscr{F}\left\{D\frac{\partial^2 P(\xi,t)}{\partial r^2}\right\} = -k^2 D\tilde{P}(k,t)$$

or, a little tidier,

$$\frac{\mathrm{d}\tilde{P}(k,t)}{\mathrm{d}t} = -k^2 D\tilde{P}(k,t)$$

This is a first order equation with solution

$$\tilde{P}(k,t) = \tilde{P}(k,0)e^{-k^2 Dt}$$

The solution $P(\xi,t)$ is then obtained by inverse transform:

$$P(\xi,t) = \mathscr{F}^{-1}\left\{\tilde{P}(k,0)e^{-k^2 Dt}\right\} = \frac{1}{\sqrt{4\pi Dt}}e^{-\xi^2/4Dt} \tag{2.8}$$

with initial condition $P(0,0) = \delta(\xi)$. The solution to eq. 2.8 might be found using Green's functions and the appropriate Green-function may be found in [17].

The isotropic diffusion of a molecule from a point ξ is then seen to be symmetrical and have a Gaussian shape, signifying the random form of Brownian motion. As the Gaussian distribution is a probability density function, the mere shape supports that self-diffusion is a random process.

The solution in terms of number density, mass density or concentration may then be expressed as

$$\bar{n}(\mathbf{r},t) = \frac{\bar{n}_0}{(4\pi Dt)^{3/2}} e^{-\mathbf{r}^2/4Dt} \tag{2.9a}$$

$$\rho(\mathbf{r},t) = \frac{\rho_0}{(4\pi Dt)^{3/2}} e^{-\mathbf{r}^2/4Dt} \tag{2.9b}$$

$$c_i(\mathbf{r},t) = \frac{c_{i,0}}{(4\pi Dt)^{3/2}} e^{-\mathbf{r}^2/4Dt} \tag{2.9c}$$

when ξ is generalized to $\mathbf{r}$ for the sake of consistency. As this is a generalization from one to three dimensions, the pre-exponential scaling factor must be raised to the power of three. The coefficients $\bar{n}_0, \rho_0$ and $c_{i,0}$ are taken to be the initial conditions.

The root-mean-square (rms) distance a molecule travels in the time t is defined as

$$\xi_{rms}(T,t) = \sqrt{\langle \xi^2 \rangle} = \left(\int_{-\infty}^{\infty} \xi^2 P d\xi \right)^{\frac{1}{2}} = \sqrt{2D(T)t} \tag{2.10a}$$

where T is absolute temperature. When generalized to three dimensions:

$$r_{rms}(T,t) = \sqrt{6D(T)t} \tag{2.10b}$$

2.1.3 The Arrhenius-type Equation

The temperature dependency of the diffusion coefficient is frequently found to be described by an Arrhenius-type equation, [25];

$$D(T) = D_0 e^{-\Delta E/RT} \tag{2.11}$$

with R being the gas constant and D_0 is a pre-exponential factor, which can be viewed as a limiting diffusion coefficient in the limit $T \to \infty$. The term ΔE is the activation energy for the process [16].

Equation 2.11 is usually valid for solids and liquids. For liquids, the concept of an activation energy is not well-defined, and should be regarded as a *pseudo* activation energy. For a liquid, it is perhaps better to interpret it as a rate limiting property of the diffusion, as listed in table 2.1, as it is then the parameter defining the three different magnitude regimes of diffusion.

Table 2.1: Regimes of diffusion depending on the ratio $\Delta E/RT$.

Thermal energy regime		**Diffusion regime**
$RT \gg \Delta E$	$\Longrightarrow$	$D(T) \approx D_0$
$RT \approx \Delta E$	$\Longrightarrow$	$D(T) \approx D_0/3$
$RT \ll \Delta E$	$\Longrightarrow$	$D(T) \ll D_0$

2.1.4 Convection

The term convection is used about mass transport in a system due to temperature gradients, ∇T. While some authors uses convection as the cumulative transport due to the bulk motion of the fluid and the Brownian motion displayed by the molecules of the sample, [26], the term will here be used only for the bulk transport of the fluid, in accordance with [23].

In fluid mechanics, convection is usually discussed in terms of the Rayleigh number, Ra. The Rayleigh number is a dimensionless number that is the product of the Prandtl number, Pr, and the Grashof number, Gr, [23];

$$\mathrm{Ra} = \mathrm{Pr} \cdot \mathrm{Gr} \tag{2.12}$$

where the Prandtl number Pr is a characteristic property of a compound, defined as the kinematic viscosity, ν, over the thermal diffusion coefficient, κ so that $\mathrm{Pr} = \nu/\kappa$.

The Prandtl number is therefore the ratio of momentum diffusivity to thermal diffusivity. As the Prandtl number includes no variables, only compound parameters, it may be regarded as a compound parameter itself.

The general significance of the Grashof number is the ratio of buoyancy to viscous forces acting on the fluid, implying that the Rayleigh number is the ratio of the buoyancy-driven flow to the thermal flow. When the Rayleigh number exceeds a critical value, the heat transport is primarily in the form of convection. When the Rayleigh number is below the critical value, the heat transport is in the form of heat conduction. If $\nabla T = \mathbf{0}$, there is no heat transport. The critical Rayleigh number, Ra_c, is estimated to, [27];

$$\mathrm{Ra}_c \approx 1708$$

and gives the limit at which the viscous forces balances the buoyancy.

The Grashof number, needed for determining the Rayleigh number, is dependent on the geometry of the problem. For a NMR tube, the problem is a 2D problem, as the flow in each point may be assumed dependent on the vertical position along the NMR tube, z and the distance from the center, r.

If there exist a dominating length scale L, the Grashof number for this geometry is given as, [23];

$$\mathrm{Gr} = \frac{g\alpha\Theta L^3}{\nu^2} \tag{2.13}$$

where g is the acceleration due to gravity, α is the coefficient of thermal expansion, L is the characteristic length of the geometry and Θ is the characteristic

temperature difference. Here, L is given by the sample height. The assumption that there is a dominating length scale is necessary in order to ignore temperature variation in other directions and assume a problem on an 1D form. Here, it is therefore assumed that the temperature only varies with z and not with r. This gives the Rayleigh number as:

$$\mathrm{Ra} = \frac{g\alpha\Theta L^3}{\nu\kappa} \tag{2.14}$$

The assumption that the convection is described in terms of the Rayleigh number holds as long as the temperature difference $\Delta T < \Delta_c T$ where $\Delta_c T$ is a critical temperature difference. When $\Delta T < \Delta_c T$, the flow is in form of Bénard flow, which is a circular flow from the bottom of the tube to the top of the tube as the hotter liquid rises. As the liquid cools, it sinks, giving the flow pattern of Bénard flow a time-independent profile as the flow pattern in a given point in the fluid does not change with time, [28]. At $\Delta T > \Delta_c T$, this flow is dominated by turbulent motion, leading to a non-symmetric flow and a time-dependent flow pattern no longer well-described by the Rayleigh number [29].

2.2 Concepts from Nuclear Magnetic Resonance Theory

2.2.1 The Magnetization Vector

The various experiments in NMR relies on perturbing the macroscopic magnetization vector, $\mathbf{M}$;

$$\mathbf{M} = \sum_i \mathbf{m}_i = V^{-1} \int_{\mathrm{V}} \mathbf{m} \, \mathrm{d}^3\mathbf{r} \tag{2.15}$$

where $\mathbf{m}$ is the magnetic moment of a spin particle by application of radio-frequency pulses acting with a torque on the magnetization vector. As the experimental method used for this thesis was ^{1}H-NMR, the spin properties of the proton is of particular interest.

If an ensemble of protons is placed in an external magnetic field, the spin orientation will be divided into two states, one along the external $\mathbf{B}$-field and one in opposition to this field [2].

This population difference between the two states turns out to follow the Boltzmann distribution, [2];

$$\frac{N_\alpha}{N_\beta} = e^{-\Delta E/k_B T} = e^{-\hbar\gamma B/k_B T} \tag{2.16a}$$

or

$$N_{\alpha/\beta} = N_0 e^{\mp\hbar\gamma B/2k_B T} \tag{2.16b}$$

where α denotes the state along the $\mathbf{B}$-field, and β denotes the state in opposition to the $\mathbf{B}$-field. The constant $\hbar$ is the reduced Planck constant. The total number of spin particles is denoted N_0, and $N_{\alpha/\beta}$ denotes the population of the α or β state.

The population difference between the two states then becomes

$$\Delta N = N_\alpha - N_\beta = N_0 e^{\hbar\gamma B/2k_B T} - N_0 e^{-\hbar\gamma B/2k_B T} \tag{2.17}$$

where the exponent may be expanded as a first-order Taylor series under the assumption that $k_B T >> \hbar\gamma B$ such that

$$\Delta N = N_\alpha - N_\beta \approx \frac{N_0}{2}\left(1 + \frac{\hbar\gamma B}{2k_B T}\right) - \frac{N_0}{2}\left(1 - \frac{\hbar\gamma B}{2k_B T}\right) = \frac{N_0 \hbar\gamma B}{k_B T} \tag{2.18}$$

gives the population difference as a function of temperature in a magnetic field. The magnitude of the magnetization vector $\mathbf{M}$ is proportional to

ΔN. The assumption that $k_B T >> \hbar\gamma B$ is usually valid under normal experimental conditions. This population splitting is called the Zeeman-splitting, [2].

2.2.2 The Bloch-Torrey - equation

The phenomenological equation for the behavior of the magnetization vector is given by Bloch, [8], and Torrey, [9], as:

$$\dot{\mathbf{M}} = \underbrace{\gamma\mathbf{M}\times\mathbf{B}}_{\text{Free precession}} \underbrace{-\left(\frac{M_x}{T_2}\mathbf{i}+\frac{M_y}{T_2}\mathbf{j}+\frac{M_z-M_0}{T_1}\mathbf{k}\right)}_{\text{Relaxation}} + \underbrace{D\nabla^2\mathbf{M}}_{\text{Diffusion}} \tag{2.19}$$

where the dot denotes time derivative, M_i are the components of the magnetization vector and M_0 is the magnitude of the magnetization vector at $t = 0$. The time constants T_i are reviewed in section 2.2.4 and 2.2.5, and T_1 is known as the longitudinal relaxation time and T_2 as the transverse relaxation time. The braces under each term is what the process in each term is conventionally named. Each process is typically measured experimentally by preparing the sample such that all other terms vanish. These processes will be reviewed further in the following sections. Equation 2.19 is conventionally named the Bloch-Torrey–equation (BTE). The components of the magnetization and the magnetic field are generally dependent on time and spatial coordinates.

2.2.3 Free Precession

For a system of spins exposed to an external, constant magnetic field $\mathbf{B}_{\text{ext}} = B_{\text{ext}}\mathbf{k}$, the BTE simplifies to

$$\dot{\mathbf{M}} = \gamma\mathbf{M}\times\mathbf{B}_{\text{ext}} \tag{2.20}$$

as no relaxation processes takes place and $\mathbf{M}$ is assumed to be time-dependent only, thus ignoring diffusion.

The direction of $\mathbf{B}_{\text{ext}}$ is set as direction for the z-component in the laboratory frame of reference.

In order to solve this partial differential equation (PDE), with $B_{\text{ext}} = B_0+\omega/\gamma$ with ω being the angular velocity of the magnetization vector and γ being the gyromagnetic ratio. Here, B_0 is the static part of the external field, while the term ω/γ is the result of the precession motion of the magnetization vector.

The cross product then becomes:

$$\dot{\mathbf{M}} = \gamma \mathbf{M} \times \mathbf{B}_{\text{ext}} = \gamma \left(M_y B_{\text{ext}} \mathbf{i} - M_x B_{\text{ext}} \mathbf{j} + 0\mathbf{k} \right)$$

and as there is no z-component, this may be written $M^+ = M_x + \imath M_y$ so the equation rewrites as:

$$\dot{M} = -\gamma M^+ B_{\text{ext}} \tag{2.21}$$

with solution

$$M_x = \Re \left\{ M^+ \right\} = M_0 \cos(\gamma B_{\text{ext}} t) \tag{2.22a}$$
$$M_y = \Im \left\{ M^+ \right\} = M_0 \sin(-\gamma B_{\text{ext}} t) \tag{2.22b}$$

or

$$M^+ = M_x + \imath M_y = M_0 e^{-\imath \gamma B \text{ext} t} \tag{2.23}$$

If presented in the rotating frame of reference, it is enough to set

$$\omega \to -\gamma B_0 \quad \therefore \quad M^+ = M_0$$

The rotating frame of reference will be used hereafter in order to simplify the different solutions to the BTE. The transform

$$\omega = -\gamma B \tag{2.24}$$

is known as the Larmour frequency, and gives the resonance frequency for a spin particle in a magnetic field [2].

In experimental settings, the signal is usually obtained in the form of eqs. 2.22a and 2.22b. One way to obtain a non-complex signal is to take the modulus of the signal. Alternatively, the largest part can be used if much larger than the other. When the latter is true, the signal is said to be "on resonance".

2.2.4 Longitudinal Relaxation

The first time-parameter in the BTE, T_1, is known as the spin-lattice relaxation time or the longitudinal relaxation time. The latter will be used in this thesis. The inverse is known as the spin-lattice relaxation rate and is denoted $R_1 \equiv 1/T_1$.

The physical interpretation of the longitudinal relaxation time is that it is the characteristic time for the z-components of the magnetization vector $\mathbf{M}$ to return to the Boltzmann-distributed state when perturbed from the Zeeman-splitting by the application of r.f.-pulses, as seen by solving eq. 2.19, with appropriate boundary conditions [30].

2.2.5 Transverse Relaxation

The second time-parameter in the BTE, T_2, is known as the spin-spin relaxation time, or the transverse relaxation time. The latter will be used in this thesis. The inverse of T_2 is sometimes used and referred to as the longitudinal relaxation rate and denoted $R_2 \equiv T_2^{-1}$.

The physical interpretation of the transverse relaxation time is that it is the characteristic time for the xy-components of the magnetization vector $\mathbf{M}$ to return to a state of zero magnitude in the xy-plane, as the spins turn to a state of randomized orientation when they are no longer subject to the Zeeman-splitting induced by the external magnetic field, as seen by solving eq. 2.19 with appropriate boundary conditions.

It can be shown that for compounds dominated by dipole-dipole relaxation, $T_1 = T_2$ [30].

2.2.6 Single-Spin and Multi-Spin Systems

If the local Larmour frequency for a spin particle is the same for all spin particles of the same kind in a compound, the compound is said to be a single-spin system. All single-spin systems are characterized by a single longitudinal and transverse relaxation time.

If the compound is characterized by more than one longitudinal and transverse relaxation time, the compound is said to be a multi-spin system. The reason why multi-spin systems have more than one relaxation time is that the local magnetic field is dependent on the magnetic field from the chemical environment.

On low-field NMR instruments, some multi-spin systems may be approximated as single-spin systems as the resonance frequencies may not be sufficiently separated. In this thesis, this approximation have been applied to 1-pentanol and tetrahydrofuran (THF).

2.3 Relaxation Mechanisms

In the following sections, the relaxation mechanisms present in the compounds that were used in the experimental work are reviewed. Although the effect of locally varying magnetic fields due to chemical environment, that is, chemical shift-anisotropy, gives rise to relaxation, it is negligible compared with the mechanisms discussed below and therefore omitted.

2.3.1 Dipole-Dipole Relaxation

The relaxation mechanism present in all compounds that were studied is the dipole-dipole relaxation, caused by the interaction between the dipole moments. As the dipole moment decay as

$$|\mathbf{m}_d(\mathbf{r})| \propto \gamma\hbar r^{-3}$$

and the dipole-dipole relaxation mechanism is a short-range interaction, decaying as

$$|\mathbf{m}_d \cdot \mathbf{m}_d| \propto \gamma^2\hbar^2 r^{-6}$$

As the magnetic moment is proportional to the gyromagnetic ratio, the effect is most prominent in ^{1}H-NMR, as it has the largest known gyromagnetic ratio. The effect of coupling between protons and other nuclei may therefore be neglected. For distances over ca. 0.5 nm, the interaction is practically negligible. The effect occurs both as intra- and intermolecular interactions, [2].

2.3.2 Relaxation by J-Coupling

The relaxation due to indirect dipole-dipole coupling through bonding electrons is known as J-coupling. To a good approximation, J-coupling is an intramolecular effect, and may be characterized by the J-coupling constant between the coupled spin particles. As J-coupling perturbs the relaxation process, compounds with J-coupling will not have the same behavior as those whose relaxation process is dominated by dipole-dipole coupling, [2].

2.4 Signal Forms

The dipole-dipole coupling and J-coupling will, in a perfectly homogeneous magnetic field, yield a relaxation time unique for a spin particle in a given chemical environment, as the effect from dipole-dipole and J-coupling stems from the transfer of magnetic moment between spin particles. This is used in structural NMR to investigate the structure and coupling scheme of organic molecules, [31].

If the external magnetic field is inhomogeneous, this will yield a spatial dependency of the local magnetic field, giving a spatial dependency of local Larmour frequencies as $\omega(\mathbf{r}) = -\gamma B(\mathbf{r})$. The FID, Hahn echo and CPMG experiments are all sensitive to inhomogeneities, as the spatial dependency of the Larmour frequencies affects the apparent relaxation rate, [32, 17].

For 1-pentanol, which might be approximated as a two-spin system for a low-field instrument as used in this work, the effect of J-coupling must also be taken into consideration. It can be shown that J-coupling in inhomogeneous magnetic fields lead to a modulation of the form

$$\frac{1}{T_2^*} = \frac{1}{T_2} + \Delta_\infty\Big(1 - \mathrm{sinc}\big(\pi J\big)\Big) \tag{2.25}$$

with J being the scalar coupling constant for the two spins, Δ_∞ is the limiting relaxation rate without the zero-correction $1/T_2$, and T_2^* is the apparent longitudinal relaxation time [33]. The sinc-function is defined as $\mathrm{sinc}(y) = \sin(y)/y$.

2.4.1 The Free Induction Decay in a Linear Magnetic Field

When dealing with the FID, generalization of the signal model was deemed necessary. A generalization taking the magnetic field inhomogeneities into account follows.

Starting with the normalized FID-signal in the laboratory frame of reference:

$$\hat{M}(t) = e^{-\frac{t}{T_2} - \imath\gamma B t} \tag{2.26}$$

and assuming $B = B(z)$ to have a linear dependency such that it may be approximated by its first order Taylor expansion

$$B(z) = \sum_{n=0}^{N} \frac{1}{n!} \left.\frac{\partial^n B}{\partial z^n}\right|_{z=0} = B(0) + \frac{\partial B}{\partial z} z \equiv B(0) + G_1 z \tag{2.27}$$

and by gauge invariance $B(0)$ may be defined as $B(0) \equiv 0$. As 2.26 now depends on both z and t, the time-dependent signal may be retained by averaging z out:

$$\begin{aligned} \hat{M}(t) &= \Big\langle \hat{M}(z,t) \Big\rangle \\ &= L^{-1} \int_0^\ell e^{-\frac{t}{T_2} - \imath\gamma G_1 z t} \mathrm{d}z \end{aligned} \tag{2.28}$$

with L as the total sample height. By the transform $\zeta = z - L/2$, yielding $\mathrm{d}\zeta = \mathrm{d}z$, and the integral taken between the boundaries $\pm L/2$, the integral

in eq. 2.28 takes the form

$$\begin{aligned}\hat{M}(t) &= L^{-1}\int_{-L/2}^{L/2} e^{-\frac{t}{T_2}-\imath\gamma G_1\zeta t}\mathrm{d}\zeta \\ &= \frac{e^{-t/T_2}}{-\imath\gamma LG_1 t}\left[e^{-\imath\gamma G_1\zeta t}\right]_{-L/2}^{\ell/2} \\ &= \frac{e^{-t/T_2}}{-\imath\gamma LG_1 t}\left(e^{-\imath\gamma G_1 Lt/2} - e^{\imath\gamma G_1 Lt/2}\right) \\ &= \frac{e^{-t/T_2}}{-\imath\gamma LG_1 t}2\imath\sin\left(-\gamma G_1 Lt/2\right) \end{aligned} \tag{2.29}$$

where the complex definition of the sine-function is used;

$$\sin(\theta) = \frac{e^{\imath\theta} - e^{-\imath\theta}}{2\imath}$$

The solution then appears as

$$\hat{M}(t) = e^{-t/T_2}\mathrm{sinc}\left(\gamma G_1 tL/2\right) \tag{2.30}$$

The negative sign is canceled as the sinc-function is an even function.

This model does not take diffusion into account, only the magnetic field inhomogeneities. An example of how to take diffusion into account is given in [10]. This model has not been used here as it is outside the scope of this thesis and the derived model proved sufficient.

2.4.2 Inversion Recovery-Signal

Solving eq. 2.19 with the boundary conditions

$$M(0) = -1 \qquad \text{and} \qquad M(t\to\infty) = 1$$

the solution is found to be

$$\hat{M}(t) = 1 - 2e^{-t/T_1} \tag{2.31}$$

with $\hat{M}(t) = M(t)/M(0)$. The longitudinal relaxation time, T_1, may then be obtained by fitting the data to a 3-parameter model

$$M(t) = A - Be^{-t/T_1} \tag{2.32}$$

without restricting the values of A or B as the condition $A = 2B$ is not always met. This is usually due to $\tau_{\min}$ being too long or $\tau_{\max}$ being too short, or a combination. Here, τ is the time values used during the experiments to build the recovery curve. The signal may also be affected by the r.f.-pulses, which are highly inhomogeneous themselves.

2.4.3 Hahn Echo-Signal

The Hahn Echo *experiment* is described in the following chapter. For now, only the retrieved signal will be discussed.

The signal from the Hahn echo experiment takes the form, [32];

$$\hat{M}(\tau) = e^{-2\tau/T_2} e^{-2D\left(\gamma\frac{\partial B}{\partial z}\right)^2\tau^3/3} = e^{-2\tau/T_2} e^{-2D(\gamma\frac{\partial B}{\partial z})^2\tau^3/3} \tag{2.33}$$

where $\hat{M}(\tau) = M(\tau)/M(0)$ is the normalized intensity and τ is the time between pulses, and $\frac{\partial B}{\partial z}$ is the effective gradient. It is assumed that $\partial B/\partial z = G_1$, that is, a linear gradient.

The experiment is then repeated with a new value of τ. Applying a list of τ-values gives the resulting Hahn echo-curve.

The term including the diffusion coefficient D stems from the varying Larmour frequency as B has a spatial dependency.

2.4.4 CPMG-Signal

As the CPMG–experiment is essentially a successive sequence of Hahn echoes with equal inter-time spacing, the signal of a CPMG–experiment composed of N echoes takes the form

$$\begin{aligned}\hat{M}(t = 2N\tau) &= \prod_n^N e^{-2\tau/T_2} e^{-2D(\gamma\frac{\partial B}{\partial z})^2\tau^3/3} \\ &= e^{-2N\tau/T_2 - 2ND(\gamma\frac{\partial B}{\partial z})^2\tau^3/3} \\ &= e^{-t/T_2 - tD(\gamma\tau\frac{\partial B}{\partial z})^2/3} = e^{-t/T_2^*}\end{aligned} \tag{2.34}$$

when the echo time $t = 2N\tau$ is introduced. The apparent transverse relaxation time T_2^*, observed experimentally, then takes the form:

$$\frac{1}{T_2^*} = \frac{1}{T_2} + \frac{D}{3}\left(\gamma\tau\frac{\partial B}{\partial z}\right)^2 \tag{2.35a}$$

or equivalently, introducing the transverse relaxation rate $R_2 = 1/T_2$ and by assuming a linear dependency in B, the apparent relaxation rate takes the form:

$$R_2^* = R_2 + \frac{D}{3}\left(\gamma\tau G_1\right)^2 \tag{2.35b}$$

where R_2 and $\frac{1}{3}D\gamma^2G_1^2$ may be found from linear regression, identifying τ^2 as the variable.

In order to distinguish between the true and the apparent transverse relaxation time, the former is denoted T_2 and the latter T_2^*. In the absence of a gradient field, the apparent T_2^* becomes the true T_2 as $\partial B/\partial z$ approaches zero. It should be noted that T_2^* in itself has no physical significance. It is simply the sum of the inherent $1/T_2$ and the diffusion-sensitive term $\frac{1}{3}D\left(\gamma\frac{\partial B}{\partial z}\tau\right)^2$.

2.4.5 Generalizations of the CPMG-signal

So far the considered model for the CPMG-signal has been that of a linear gradient field, i.e.

$$B(z) = B(0) + G_1 z$$

where effects of vertical translation may be ignored as any vertical translation and sample geometry might be removed due to the gauge invariance of $B(0)$.

A proposed model, accounting for a second-order gradient field must take the geometry of the sample tube into consideration, as some NMR-tubes have a hemisphere end and therefore yields a smaller signal due to the reduced amount of sample in this part of the tube. The proposed model is, [19];

$$\begin{aligned}\frac{1}{T_2^*} &= \frac{1}{T_2} + \frac{D\gamma^2 G_1^2}{3}\left((1+2k\ell) + \frac{6-\rho^2}{3-\rho}k(1+2k\ell)L + \frac{4-\frac{2}{5}\rho^3}{3-\rho}k^2L^2\right)\\ &= \frac{1}{T_2} + \frac{D\gamma^2 G_1^2}{3}K(k,\ell,L,\rho)\end{aligned} \tag{2.36}$$

with ℓ being the vertical shift of the NMR tube from a reference position along the z-axis, L being the total sample height, and $k = G_2/G_1$ is the ratio between the second- and first-order term in the assumed form of the magnetic field. The parameter $\rho = r_0/L$ is the ratio between the radius of the hemisphere, r_0, and the total sample height. The sum within the large parenthesis may be written as a correction function $K(k,\ell,L,\rho) = (1+2k\ell) + \frac{6-\rho^2}{3-\rho}k(1+2k\ell)L + \frac{4-\frac{2}{5}\rho^3}{3-\rho}k^2L^2$. A simplified version is derived in appendix D on page 99, assuming a cylindrical geometry for simplicity and $\ell = 0$.

Chapter 3

Methods

This chapter reviews the experiments used together with a short discussion of the treatment of the obtained data.

3.1 NMR Pulse Sequences

This section describes the various NMR-pulse sequences used in this work.

As the NMR-instrument is a well-established instrument, the description of the instrumental set-up is omitted in this thesis. The interested reader is referred to [2].

3.1.1 The Free Induction Decay

The free induction decay experiments consists of a single r.f.-pulse designed to flip the magnetization vector from the equilibrium state parallel to the external **B**-field into the xy-plane, [2]. This type of pulse is denoted a $\frac{\pi}{2}$-pulse. As the spins are no longer subject to the Zeeman-splitting, the magnetization decays as the spins dephase in the xy-plane. It is the measurement of this decay that gives the FID-signal. This is the previously mentioned transverse relaxation.

A sketch of the FID pulse sequence is provided in fig. 3.1. In this figure, and the subsequent provided, the gray block denotes a r.f.-pulse and the following curve denotes the signal. The subscripts x and y are used to denote along which axis the pulse is applied, so a $\left(\frac{\pi}{2}\right)_x$-pulse is applied to flip the magnetization in the x-direction. If this pulse is followed by a π_y-pulse, the magnetization is reflected around the y-axis into the $-x$ axis. For more complicated pulse-sequences, such as the CPMG-experiment, the direction of the pulses are usually alternated when repeated in order to avoid a build-up effect if the applied pulses used are non-uniform. This is known as phase

cycling, and is omitted from the rest of this thesis. See [2] for further reading.

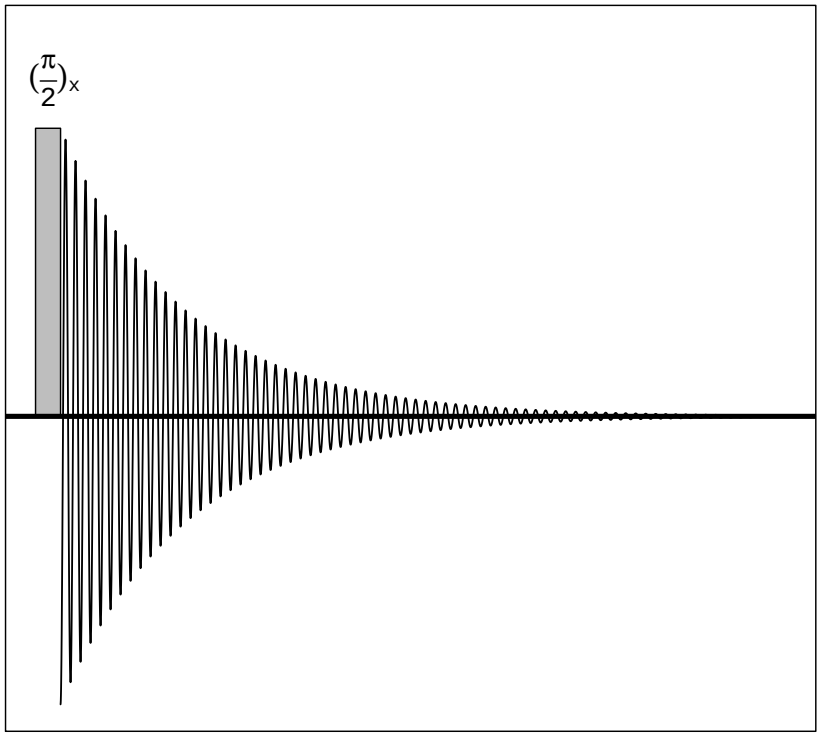

Figure 3.1: A sketch of the free induction decay (FID)–experiment.

Sometimes, the FID-experiment is used to estimate T_2. As documented in section 5.2, this should be avoided unless performed using an instrument with the opportunity for shimming the applied magnetic field, as shimming is used to minimize magnetic field inhomogeneities.

Another issue with estimating T_2 from the FID is that there is a time interval between the end of the pulse and the when detector coil starts to detect the signal. This is due to the strong electrical currents induced in the coil by the r.f.-pulse. Therefore, there is a time delay between the two events, in order for the currents to die out. In this time interval, valuable information about the initial form of the the signal may be lost for systems with short

T_2 in form of the initial intensity, which makes this form of estimation of T_2 even more flawed.

3.1.2 The Inversion Recovery–Experiment

The inversion recovery–experiment consists of a π-pulse that inverts the magnetization vector before relaxation takes place. After a time τ, a $\frac{\pi}{2}$-pulse is applied in order to flip the remaining magnetization into the xy-plane where the remaining magnetism is detected. The experiment is then repeated with different values of τ in order to build a so called inversion recovery curve, [2]. A sketch of the experiment is provided in fig. 3.2.

The experiment is used to estimate T_1, which is then used for estimating the repetition delay between successive experiments. The repetition delay is the waiting time between two successive experiments in order to establish a magnetization vector to use during the experiment. Consensus is to use a repetition delay equal to $5T_1$, although sometimes $3T_1$ is used. The former recover ≈ 99 % of the magnetization and the latter ≈ 95 %, assuming the magnetization to be recovered lies somewhere in the xy-plane.

In the case of the inversion recovery–experiment, the signal initially has a negative magnitude. When working with the modulus of the signal, the correct form of the signal is retained if the sign of the signal is set to be the same as the part with largest magnitude. The real part usually has the largest magnitude.

An algorithm for determining values of τ in order to ensure an evenly spaced recovery-curve is given in appendix A on page 85.

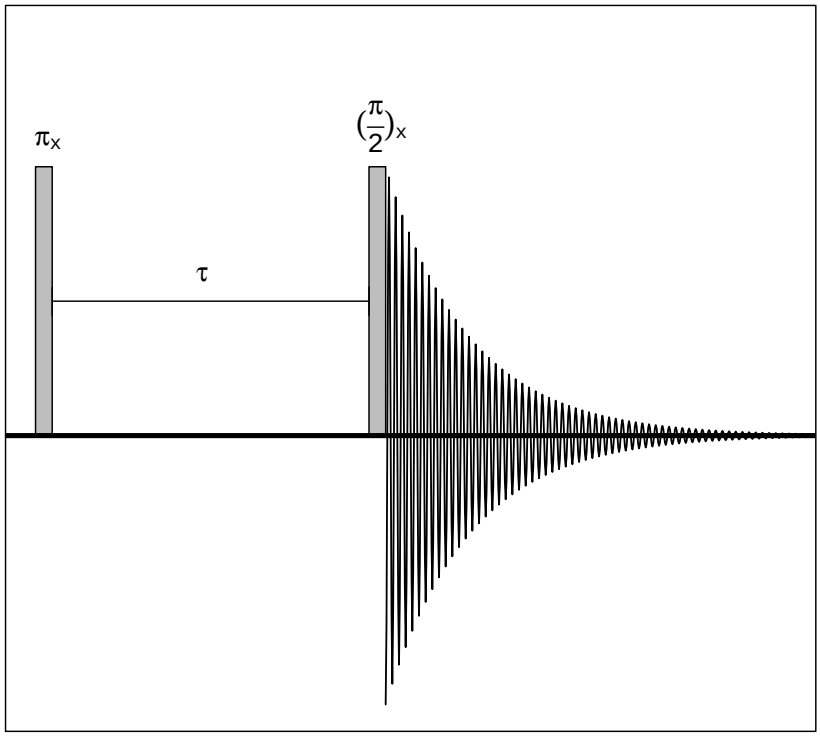

Figure 3.2: A sketch of the inversion recovery–experiment.

3.1.3 The Hahn Echo–Experiment

The Hahn Echo-experiment consists of a r.f.-pulse that flips the magnetization vector into the xy-plane, much like the FID-experiment, and allowing the magnetization to dephase for a time τ. After the a dephasing time τ, a r.f.-pulse is applied, reflecting the magnetization through the yz-plane, [3]. As the magnetization will dephase as mentioned in section 3.1.1, the reflection causes the magnetization to refocus at time 2τ from the first pulse, yielding a spin echo. Then, the experiment is repeated with an increased value of τ. A sketch is provided in fig. 3.3.

The phenomenon of the spin echo has its origin in the transverse relaxation process discussed in section 2.2.5 on page 15. The phenomenon is observed when an ensemble of spin particles is placed in an external magnetic field $\mathbf{B}$ and subjected to an r.f.-pulse that flips the spin an angle of $\pi/2$ radians into the plane normal to $\mathbf{B}$. The angle might be different from $\pi/2$ and still produce an echo, as the component along the measuring coil will be detected. As T_2 is a characteristic time for the spins to dephase, the reflecting pulse causes the spins to refocus, and this refocusing gives the measurable signal called the Hahn echo, in recognition of its discoverer, Erwin Hahn.

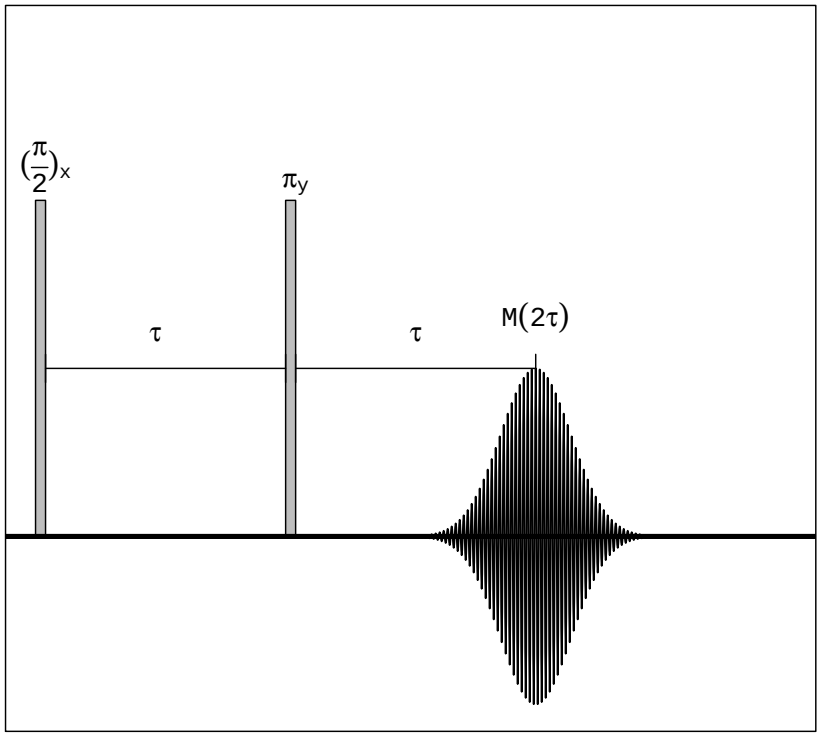

Figure 3.3: A sketch of the Hahn Echo–experiment.

3.1.4 The CPMG–Experiment

The CPMG-experiment consists of a sequence of Hahn echoes with fixed τ, [4, 5]. The echo is sampled after each π-pulse, before applying another π-pulse. A sketch of the CPMG-pulse sequence is given in fig. 3.4. In this figure, "loop" is used to denote the sequence of π-pulses.

As the retrieved echo is sensitive to diffusion, CPMG is frequently used to detect diffusion when working with various porous systems where the magnetic field inhomogeneities are introduced by the susceptibility differences between fluid and the solid matrix, [6, 7].

The scope of this thesis has been to determine whether or not a parameter $G_1^2 = \left(\frac{\partial B}{\partial z}\right)^2$ is independent of temperature and sample, and if so whether or not it can be used to estimate the diffusion coefficient D by CPMG, as this can be done on a basic NMR instrument, provided the magnetic field is sufficiently inhomogeneous.

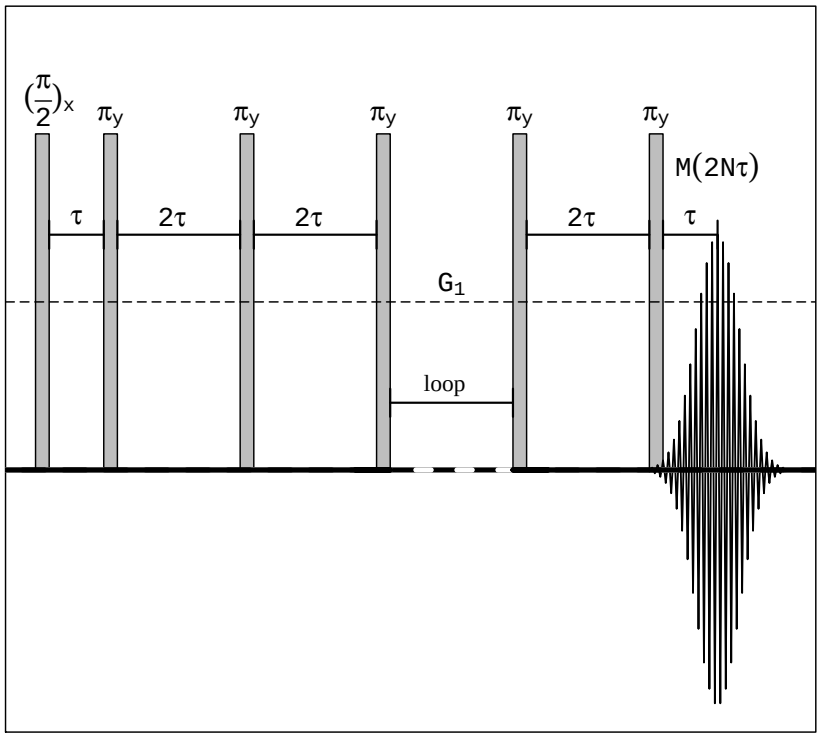

Figure 3.4: A sketch of the Carr-Purcell-Meiboom-Gill (CPMG)–experiment.

3.2 Modeling and Numerical Analysis

All data analysis has been done using the scripting language `R` . A comprehensive overview of `R` is given in reference [34].

3.2.1 Nonlinear Regression

The `nls()`-package in `R` was used for processing the signals from the CPMG-experiments. The `nls()`-package uses the Gauss-Newton–algorithm (GNA) in order to estimate the best set of parameters for a given model to a given data set [35]. The script used to analyze the CPMG data is in reviewed in appendix C on page 93.

Various textbooks and literature often estimates the parameters for a nonlinear model by mapping the nonlinear problem to a linear one before applying linear regression and then mapping back to the original problem, [25]. This is fine from a theoretical perspective, but there are two reasons why this practice is not optimal.

First, consider the case of a CPMG-signal,

$$I(t) = M(t) + \epsilon = M(0)e^{-t/T_2} + \epsilon$$

with $M(t)$ being the magnetization at time t, and ϵ being the noise which is assumed to be random. The total signal is denoted $I(t)$.

The transform that maps the above equation to a linear problem is simply the natural logarithm, and the resulting mapping of the magnetization is then

$$\ln(M(t)) = \ln(M(0)) - \frac{t}{T_2} = a + bt$$

However, for the total signal, the mapping becomes

$$\ln(I(t)) = \ln\left(M(0)e^{-t/T_2} + \epsilon\right) \approx \ln(M(t)) + \sum_{n}^{\infty} \frac{1}{n}\left(\frac{\epsilon}{M(t)}\right)^n$$

where the approximation is a Taylor expansion around $\epsilon \approx 0$. A first-order approximation is then

$$\ln(I(t)) \approx \ln(M(0)) - \frac{t}{T_2} + \frac{\epsilon}{M(t)}$$

which shows that the signal-to-noise ratio directly affects the estimated parameters.

The problem then becomes how, from the errors estimated for the parameter a, to account for the noise term ϵ and how to make an error estimate for the parameter estimated in the original problem, and whether or not this mapping add to the error. This is the motivation for using nonlinear regression. By not mapping the problem back and forth between a linear representation and the original representation, the noise term may be included in the model when estimating the parameter $1/T_2$ from the residual between observed data and optimized model.

The second reason is more complex. In some cases, the obtained signal is not very good. As an example, take the raw data for THF in this thesis which is presented in 5.6.7 on page 65. Neither commercial software (WinFit by NOVOCONTROL) nor the homemade script managed to find the parameters that best describes this bi-exponential model. It is then of course possible to estimate parameters from a linear mapping, dividing the the semi-logarithmic data into two subgroups followed by linear regression. This is obviously a difficult algorithm to implement, as it is difficult to split the data into two subsets *a priori*, but this argument is currently omitted as it is possible. The key point is that the use of nonlinear regression can make clear when a model does not longer fits the observed data.

The references reviewing the convergence properties of the GNA are given in appendix C. In the case for THF, where it seems impossible to find an acceptable solution to the estimation problem, the fact that no solution is obtained can be seen as a statement that the data is too flawed to fit to a simple bi-exponential model and another model should be considered for this signal. As this is contrary to existing practice, the use of nonlinear regression does in general provide a guide for when further data analysis should be abandoned.

A third minor reason, related to the previous one, is that it allows for estimating several parameters at the same time. Take the multi-exponential signal as an example. The nonlinear approach allows for estimating all parameters at once, while the linear mapping implies that the transformed data must be subdivided into different regions with the problem of not being able to decompose the noise. This last approach is difficult to automate, and is thus not suited when working with large, complex data sets.

3.2.2 Weighted Linear Regression

The estimate for the squared gradient G_1^2 was obtained from linear regression, in accordance with eq. 2.35b.

For varying values of τ, some estimated values of R_2 have a greater uncertainty than others. When using linear regression to estimate parameters, these variations may be taken into account using weighted linear regression, allowing measurements with smaller uncertainty being weighted more than those with larger uncertainty.

The weighted linear regression problem is to minimize the sum of squared residuals, SS, defined as

$$SS = \sum_{n=1}^{N} w_n \Big(Y_n - y(x_n) \Big)^2 \tag{3.1}$$

with w_n as weights. In this thesis, $w_n = \sigma_n^{-1} = (\delta R_2(\tau_n))^{-2}$ with $\delta R_2(\tau_n)$ being the standard deviation for $R_2(\tau_n)$ and σ_n is the variance. The residual is the difference between the measurements Y_n and the model y. In the case of "ordinary", unweighted, linear regression, all weights are set equal to 1. The standard deviations were computed from each set of T_2 for a given τ.

Chapter 4

Experimental Information

This chapter gives the information about the samples used, the experimental settings and the set-up of the CPMG-experiments. All other experiments were run as described in chapter 3 at 30 °C.

All experiments were run at a Maran Ultra instrument with a 0.5 T permanent magnet.

4.1 Sample preparation

All liquids used for this study are listed in table 4.1 and information regarding producer, purity and what atmosphere each sample is enclosed in are given in table 4.2. All samples except the water sample was degassed at a vacuum line. Each sample had previously been dried for a variable amount of days over molecular sieve. The degassed sample was then transferred to a NMR-tube under argon atmosphere. The tube was sealed immediately afterward. The preparation of the water sample consisted of boiling tap water before transferring it to a NMR-tube. Nitrogen gas was then bubbled through the water before the tube was sealed. This sample has been used for instrumental training for the last 10 years and the results obtained from it has proved reproducible.

The THF was taken from a MBraun MB-SPS-800 solvent dispenser and has, strictly speaking, an unknown producer and purity. It is however safe to assume the purity to be in the order 90 $\%_{\mathrm{V}}$. At this solvent machine, all solvents are stored without stabilisators.

4.2 Experimental Settings

The temperature settings were estimated using a mercury thermometer inserted into the sample cell while adjusting the temperature setting at the in-

Table 4.1: Chemical data of the samples investigated.

Sample	**Molar mass**, [36]/ **[g/mole]**	**Boiling point**, [36]/ **[°C]**	**Sample height**/ **[10^{-3}m]**
Benzene	78.11	80.1	7
Cyclohexane	84.16	80.7	10
DMSO	78.13	189	8
1-Pentanol	88.15	137.5	6
THF	72.11	66	8
Water	18.02	100	8

Table 4.2: The producer and conditions of the different liquids used in this thesis.

Compound	**Producer**	**Purity**/ **[%$_V$]**	**Atmosphere**
Benzene	Baker Analyzed	$\geq$ 99.7	Ar
Cyclohexane	Baker Analyzed	$\geq$ 99.5	Ar
DMSO	Fluka Chemie AG	$\geq$ 99.0	Ar
1-Pentanol	Fluka Chemie AG	$\geq$ 98	Ar
THF	Solvent dispenser	-	Ar
Water	-	-	N_2

strument until finding the matching temperature. These estimates were later tested with a home-made thermometer consisting of a digital temperature logger immersed into a mixture of water and glass beads in order to simulate the heating of a system with a liquid phase. This temperature logger was also used in order to estimate how long it takes for the sample to be heated from one temperature to another. This heating time was estimated to be 10 minutes and seemingly independent of start and stop temperature, [37]. During the experiments, the samples were left to heat for 25 minutes after changing temperature and before starting a new sequence of experiments. The heating time was increased in order to make sure no flows were induced during measurements.

The duration of the $\frac{\pi}{2}$-radian pulses were obtained by use of the automatic functions of the instrument and estimated to 1.95 μs. The duration of the π degree pulse was determined by multiplying the duration of the $\frac{\pi}{2}$-radian pulse by two. These automatic functions, both for determining the duration of a $\frac{\pi}{2}$-radian pulse and the receiver gain, were run three-five times after each other together with estimating the resonance frequency, in order to make up for any initially wrong estimates.

The receiver gain, RG, is the parameter scaling how large a fraction of

the total signal is detected by the hardware. Some comments on the receiver gain are made in the next section.

All estimates of experimental settings for each compound were done at $\theta = 30$ °C. The estimates for water were later tested at $\theta = 60$ °C in order to check if these parameters would change with temperature. No change in P90-duration was observed. A rise in receiver gain was observed, but as the receiver gain generally should be set lower during the CPMG-experiments than estimated by the automatic function, this setting may be left unchanged.

4.2.1 Receiver Gain-Settings

If the receiver gain is set too high, the electrical pulse which induces the signal in the measuring coil of the instruments becomes too strong. In order for the coil not to break, the signal is then blocked out. In order to avoid the signal being blocked out, the receiver gain is always set lower than the value suggested by the automatic function, as it is deemed better to have a lower signal-to-noise ratio than to take the chance of having signal blocked out as experiments were running continuously for 5-7 days at the time. The signal-to-noise ratio is therefore compromised in order to avoid unnecessary interruptions.

4.2.2 Estimated Temperature Difference

The temperature difference in the sample cell was estimated over the range of 1 cm by use of the home made temperature logger made by [37]. The estimated temperature differences at given temperatures are given in table 4.3. At 30 °C, the temperature is estimated to be larger at the top of the sample than at the bottom. The temperature-logger has two sensors, one in the bottom hemisphere and one about 1 cm above.

There is no clear reason why the temperature difference is inverted at 30 °C. As the air flow can be assumed to be faster at the bottom of the sample, as this is closer to the air outlet, this may give a cooling effect at low temperatures, much like when wind gives a lover apparent temperature.

Table 4.3: The temperature difference estimated over 1 cm of the sample cell at the experimental temperatures.

Temperature/ [°C]	**Temperature difference / [°C]**
30	-0.3
40	0.4
50	0.8
60	1.4

4.3 The CPMG-Experiments

The CPMG experiments for each compound were run at the temperatures $\theta = 30, 40, 50, 60$ °C with 22 different τ-values for each compound ranging from $\tau_{\min} = 1$ ms to $\tau_{\max} = 52$ ms, except for THF with $\tau_{\max} = 30$ ms. The τ-value list for THF had to be truncated due to instrumental limitations for compounds with long longitudinal relaxation time. As THF is a multi-spin system, it could not benefit from the method described in the next section. At each temperature, four replicates were run before changing the temperature setting. Depending on repetition delay, the experiment sequence for each compound had a total duration of five to seven days. It is due to this long total experimental time that for instance the receiver gain is set lower than the estimated value in order to avoid interruptions. This gives a total data set of $\approx$ 1600 CPMG-curves.

4.3.1 A Modified Experiment for Long Repetition Delay

It is necessary to wait a certain time interval between successive experiments, in order to recover a magnetization vector. This inter-experiment time will be denoted as the repetition delay (RD). As the RD generally is set to five times T_1, problems occur for systems with T_1 in orders of tens of seconds. In this work, this was the case for benzene (see table 5.3 on page 47). As the instrument used has limitations on the number of echoes allowed for a given RD, benzene's property of being an equivalent proton-system was exploited.

As all protons in benzene have the same chemical environment, it behaves like a single-spin system, and the long RD could be omitted and substituted for a shorter RD, allowing for sampling more echoes. The idea is to establish a steady-state magnetism and rather work with this than using the fully recovered magnetization vector. The idea is fully worked out in appendix B on page 89. The calculations in this appendix gives that the steady state magnetism is $\approx$ 66 % of the full magnetism. In contrast, a RD equal to five times T_1 recovers $\approx$ 99 %.

The equations developed in the appendix were also used for estimating how many pulses are needed in order to establish a steady-state magnetism under the given circumstances. As it appears that it was necessary with four pulses before the steady-state magnetism was properly developed, the experimental procedure was changed by adding four dummy scans before initiating each CPMG-experiment with a RD = T_1. A dummy scan is the application of a pulse without measuring the recovered magnetism.

Although the signal-to-noise ratio is compromised by the reduced magnetism, the ratio is somewhat improved due to the increased number of echo which gives a better description of the CPMG-curves.

The results from these experiments seems perfectly in line with those for water, cyclohexane and DMSO.

4.4 General Approach to Signal Treatment

As the signals measured in NMR have an oscillating form in the laboratory frame, the general form of any such signal is

$$M(t) = M^{\Re}(t) + \imath M^{\Im}(t) \tag{4.1}$$

where the real part of the signal is denoted $\Re\{M(t)\} = M^{\Re}(t)$ and the imaginary part $\Im\{M(t)\} = M^{\Im}(t)$. When performing NMR-experiments, it is normal to try to have the signal on resonance, that is, match the angular frequency of the rotating frame of reference to that of the oscillating field without any additional phase factor, as in eq. 2.24. A signal perfectly on resonance will not necessarily have an imaginary part of pure noise, as diffusion and inhomogeneities may lead to an altered phase of the signal. As the real part is usually the only significant signal, it can therefore be used alone. In the case of the Hahn echo and CPMG, the imaginary part is usually mostly random, but the modulus, i.e. $M(t) = \sqrt{\left(M^{\Re}(t)\right)^2 + \left(M^{\Im}(t)\right)^2}$ might be used in order to capture most of the curve and add an additional parameter ϵ accounting for the adjusted offset. Dependent on the estimated resonance frequency, the role of the real and imaginary part as discussed above might be interchanged.

Chapter 5

Results and Discussion

This chapter presents the results from FID and Hahn echo used to investigate the presence of magnetic field inhomogeneities. Also presented are the inversion recovery experiments used to estimate the repetition delay and the CPMG-experiments used to probe diffusion of the selected sample molecules and a sensitivity analysis. The chapter also includes a discussion of the Rayleigh number for the various experiments, diffusion coefficients from literature and values interpolated for DMSO and a discussion of the sensitivity of the parameters of the correction function $K(k, L, \ell, \rho)$.

5.1 The Presence of Magnetic Field Inhomogeneities

If the magnetic field proved to be sufficiently homogeneous, the CPMG-signal would be independent of the inter-pulse spacing τ, and all curves fall along the same straight line in a semi-logarithmic plot. Also, the FID and the CPMG should fall along the same, straight line in a semi-logarithmic plot. The presence of the magnetic field inhomogeneities can therefore be seen from figs. 5.1a and 5.1b, as it is clear that the FID signals deviate from the straight line and that the CPMG-signal is dependent on the value of τ. It is therefore clear that the magnetic field is sufficiently inhomogeneous to perform diffusion measurements by CPMG.

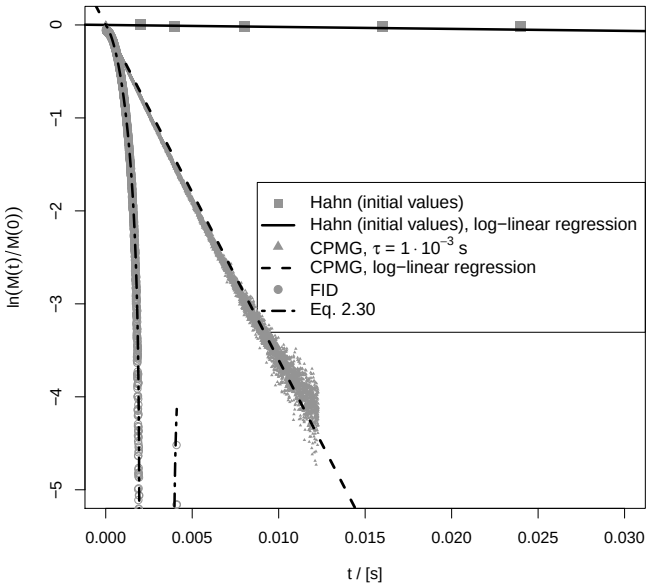

(a) The FID-, CPMG- and Hahn echo-signal. The plot is semi-logarithmic.

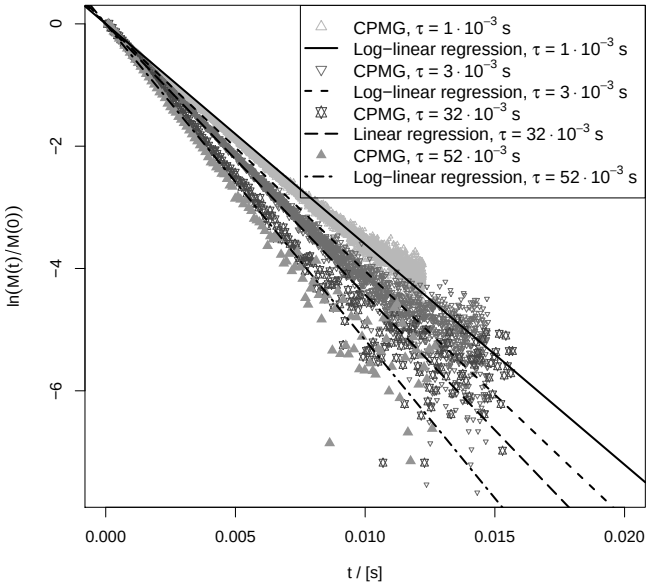

(b) CPMG-signal for various values of τ. The plot is semi-logarithmic.

Figure 5.1: The effect of magnetic inhomogeneities on the FID-, CPMG- and Hahn echo-experiment.

5.2 Free Induction Decay

A FID-signal was obtained from water to examine the effect of inhomogeneous magnetic field on the FID-signal, as shown in fig. 5.2a. By considering the raw data, it is clear that the signal may not be described by the decaying exponential predicted by solving the BTE with the imposed boundary conditions. The real part of the signal obtained was then fitted to the model equation derived by the end of chapter 2, eq. 2.30;

$$M(t) = M_0 e^{-t/T_2} \text{sinc}(L\gamma G_1 t)$$

where no form of baseline-correction has been included as the signal takes both positive and negative values. This model has been used for the regression in fig. 5.2a. As the sinc-function accounts for the inhomogeneity in the magnetic field, the parameter G_1 estimated here is due to the inhomogeneous field, and because of this it is inherently impossible to stay on-resonance, that is, fulfilling the transform $\omega = -\gamma B$ mentioned in section 2.2.3. It should be noted that the modified expression does not account for the effect of diffusion, and could be generalized further. This is however outside the scope of this study. Diffusion has been taken into account by [10]. As the scope of this experiment was to show that the magnetic field is inhomogeneous and that the FID-signal may no longer be described by a decaying exponential, the full model from [10] was not used here.

This experiments demonstrates why the FID-experiment should be avoided when estimating T_2, as it is highly sensitive to inhomogeneities. Some technical issues with using FID for estimating T_2 are mentioned by the end of section 3.1.1 on page 21.

The parameters estimated for the model are given in table 5.1. It can be seen from the residuals in fig. 5.2b that the model is not very good, as the residuals have an obvious underlying periodicity. This is most likely due to the fact that the modified expression of eq. 2.30 does not take diffusion into account and only addresses the inhomogeneity of the magnetic field. Although this might be fixed by using the full model from [10], the model used is much better than the single exponential usually used for modeling the FID-signal.

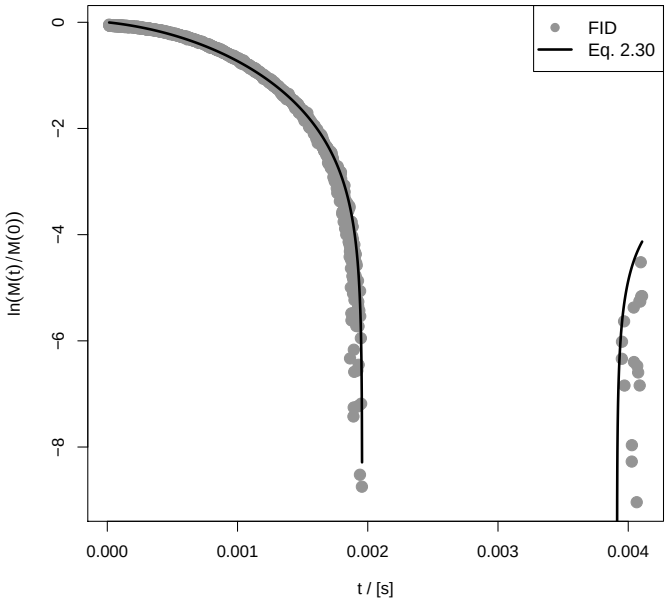

(a) The normalized FID-signal and the modified model. The plot is semi-logarithmic.

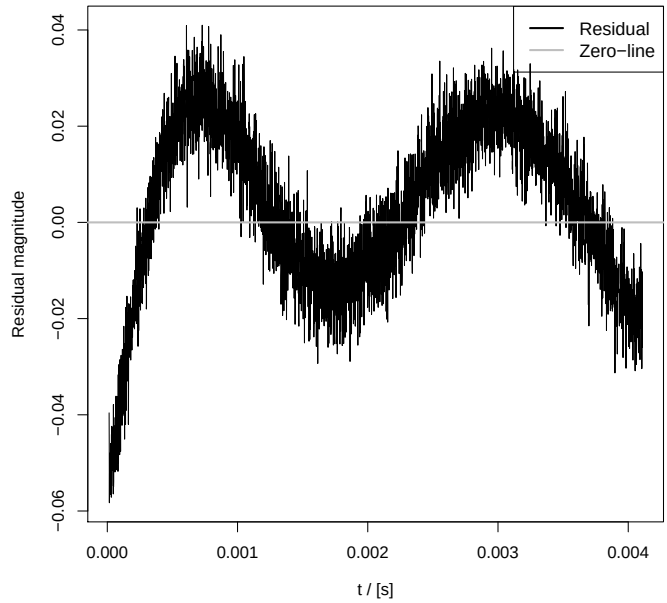

(b) Residual of the modified form of the FID-signal.

Figure 5.2: The effect of magnetic inhomogeneities on the FID-signal.

Table 5.1: Parameters estimated for the modified FID.

Parameter	**Estimate**	**Unit**
T_2	3.88 ± 0.02	10^{-3}s
G_1	9.426 ± 0.007	10^{-3} T m^{-1}

5.3 Hahn Echo

A Hahn echo-experiment was performed with water at 30 °C in order to examine the effect of magnetic inhomogeneities on the Hahn echo. As the Hahn echo should behave according to eq. 2.33, the signal was fitted to a 4-parameter equation

$$M(\tau) = M_0 \exp\left(-\frac{2\tau}{T_2} - \frac{2}{3}D\gamma^2 G_1^2 \tau^3\right) + \epsilon \tag{5.1}$$

where $G_1 = \partial B/\partial z$ and the parameter ϵ might be interpreted as the average noise and τ is the inter-pulse time. The offset-parameter ϵ was estimated to ≈ 0.5 % of M_0, pointing to an insignificant contribution. It was however added as it gives the residual a random form, rather than a linear one. The estimated G_1^2 should in theory be consistent with G_1^2 estimated from the CPMG-results. It is however estimated to be ≈ 5 times larger. This might be due to the fact that the relaxation due to diffusion is independent in each time intervall τ, which is the same reason why the diffusive term is dependent on $DG_1^2 2\tau^3/3$ and not $DG_1^2(2\tau)^3/3$ as noted in [32]. As the diffusion is independent in τ, this would lead to an over-estimation of G_1^2, when compared to the estimate by CPMG, as the time-variable in a CPMG-experiment is $t = 2N\tau$ for the N-th echo, thus leading to an implicit factor 4 being taken out with time. Thus the conversion of G_1^2 estimated from a Hahn echo must be divided by a factor 4 to account for the time-scaling. The estimated parameters of the 4-parameter equation are given in table 5.2. This is within two standard deviations of the estimate obtained from the CPMG-experiments in section 5.6.4. The fitted model is given in fig. 5.3a with the residual given in fig. 5.3b.

Table 5.2: Parameters estimated for the Hahn echo of water at 30 °C.

Parameter	**Estimate**	**Unit**
T_2	2.0 ± 0.1	s
G_1^2	127 ± 1	10^{-6} T^2 m^{-2}

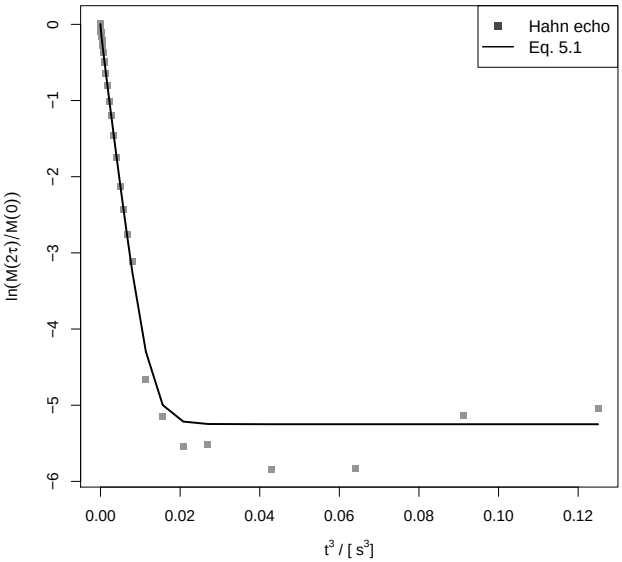

(a) The normalized Hahn echo for water at 30 °C and the fitted 4-parameter model. The plot is semi-logarithmic.

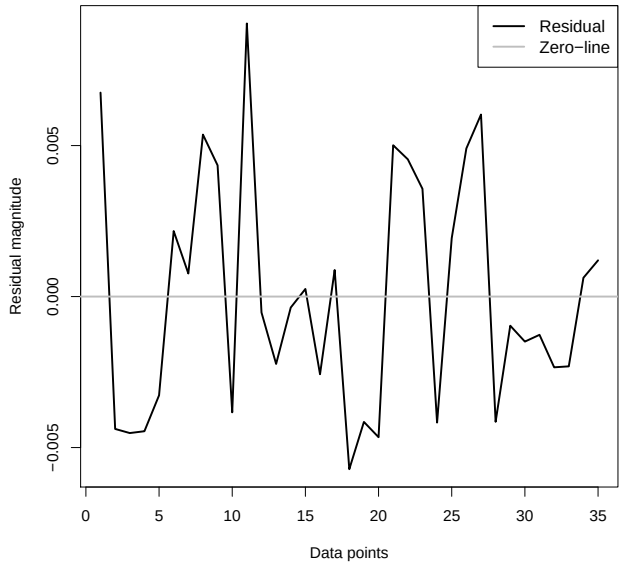

(b) The residuals of the 4-parameter model.

Figure 5.3: The effect of magnetic inhomogeneities on the Hahn echo-signal.

5.4 Inversion Recovery

A series of inversion recovery experiments were performed in order to estimate T_1, and thus RD, for the various compounds at $\theta = 30, 40, 50, 60$ °C, the temperatures used in the CPMG-experiments.

This temperature-study of the behavior of T_1 was done after the CPMG-experiments in order to check that too short RDs had not been used. In cases where RD was too short, the experiment was repeated with corrected RD unless the given molecule proved to be of no use for diffusion study by CPMG. This was the case for THF, which is why it is not included in the table below. At 30 °C, T_1 for THF was measured to $T_1 = 11.9$ s. The results for THF are reviewed in detail in section 5.6.7.

After the experiment with benzene, it was discovered that the τ-list was truncated as the instrumental software did not support sufficiently long inter-pulse times. Therefore the inversion recovery-curves were not fully developed, they were sufficient to estimate the RD for CPMG-experiments. Due to the long T_1, the benzene experiments were modified as described in appendix B.

Table 5.3: Longitudinal relaxation data obtained by inversion recovery.

Compound	**Temp / [°C]**	**T_1 / [s]**
Benzene	30	12.4 ± 0.1
Benzene	40	13.9 ± 0.2
Benzene	50	16.8 ± 0.3
Benzene	60	17.9 ± 0.4
Cyclohexane	30	3.987 ± 0.005
Cyclohexane	40	4.428 ± 0.008
Cyclohexane	50	5.088 ± 0.009
Cyclohexane	60	5.89 ± 0.01
DMSO	30	2.885 ± 0.008
DMSO	40	3.36 ± 0.01
DMSO	50	3.91 ± 0.01
DMSO	60	4.41 ± 0.02
1-Pentanol	30	1.240 ± 0.006
1-Pentanol	40	1.533 ± 0.006
1-Pentanol	50	1.914 ± 0.007
1-Pentanol	60	2.348 ± 0.008
Water	30	3.206 ± 0.007
Water	40	3.92 ± 0.01
Water	50	4.83 ± 0.01
Water	60	5.76 ± 0.03

5.5 Literature Values for the Diffusion Coefficient

In order to estimate diffusion coefficients with the outlined method, the parameter G_1^2 in the term from eq. 2.35b on page 19:

$$\frac{D}{3}\left(\gamma G_1\right)^2 \tag{5.2}$$

must be estimated. As γ is known, the only other unknown parameter is the diffusion coefficient. By use of literature values for the compounds used, the gradient field squared, G_1^2 can be estimated. When the literature values were measured at the same temperatures as those used in this work they were used directly, and interpolated when measured at different temperatures. Table 5.4 provides the diffusion coefficients from literature sources. As the values estimated by [38] have relative uncertainties one to two orders of magnitude smaller than the parameter estimated from linear regression in eq. 5.2, these uncertainties will not be considered further, as their contributions are negligible.

The diffusion coefficients for DMSO given in [25] were not measured at the same temperatures as in this work, so the diffusion coefficient was interpolated using the Arrhenius-type equation, eq. 2.11 on page 8. The diffusion coefficient at 60 °C has been extrapolated as it is outside the temperature interval used in [25].

The interpolated values are given in table 5.5 and the parameters obtained by nonlinear regression are given in table 5.6. The uncertainties were calculated from the equation

$$\delta D(T) = D(T)\sqrt{\left(\left|\frac{\partial D(T)}{\partial D_0}\right|\delta D_0\right)^2 + \left(\left|\frac{\partial D(T)}{\partial \Delta E}\right|\delta \Delta E\right)^2} \tag{5.3}$$

with

$$\frac{\partial D(T)}{\partial D_0} = \exp(-\Delta E/RT) \tag{5.4}$$

$$\frac{\partial D(T)}{\partial \Delta E} = -\frac{D_0}{RT}\exp(-\Delta E/RT) \tag{5.5}$$

when inserting eq. 2.11 to eqs. 5.4 and 5.5.

Table 5.4: Literature values for diffusion coefficients of compounds at different temperatures.

			$\mathbf{D_{lit}}$, [38]/ $[10^{-9}\mathbf{m^2 s^{-1}}]$
Temperature/ [°C]	**Benzene**	**Cyclohexane**	**Water**
30	2.45 ± 0.03	1.65 ± 0.01	2.6 ± 0.1
40	2.87 ± 0.03	1.92 ± 0.04	3.20 ± 0.04
50	3.37 ± 0.07	2.26 ± 0.04	3.89 ± 0.06
60	3.90 ± 0.08	2.63 ± 0.07	4.62 ± 0.03

Table 5.5: Interpolated diffusion coefficients for DMSO.

Temperature/ [°C]	$\mathbf{D_{int}}$ / $[10^{-9}\mathbf{m^2 s^{-1}}]$
30	0.82 ± 0.03
40	0.99 ± 0.03
50	1.19 ± 0.04
60	1.40 ± 0.04

Table 5.6: Parameters for interpolating diffusion coefficients for DMSO.

Parameter	**Estimate**
ΔE / [kJ mole^{-1}]	14.87 ± 0.09 s
D_0 / [10^{-8} m^{2}s^{-1}]	30 ± 1

5.6 CPMG

5.6.1 Model-Fitting

The raw data obtained from the CPMG-experiments was fitted to a 3-parameter-model

$$M(t) = M_0 e^{-t/T2} + \epsilon \tag{5.6}$$

as an unrestricted fit. The parameter ϵ is included as a baseline-correction and can be interpreted as an estimate of the mean noise. It seems obvious that M_0 should be the same for all CPMG-curves, independent of τ. However, as apparent relaxation curves, it seems wrong to make this constraint and that the estimates of M_0 should rather be used to check the reliability of the model. The implementation of this constraint is also non-trivial with the used software.

It is sometimes discussed whether or not to truncate the signal, as much of the total signal for a given CPMG-experiment may consist solely of noise. As the model used in this work appears to give a seemingly random residual, it appears to have no particular bias and is therefore an acceptable model. CPMG-curves for water at 30 °C, for $\tau = 1$ and 52 ms, are given in fig. 5.4a and 5.4c with corresponding residuals in fig. 5.4b and 5.4d. Although the real signal might also be used for this analysis, the imaginary part of the signals appears to be randomly distributed with zero mean, making the use of the modulus or the real part gives no significant change except for an increased baseline, here included as ϵ.

As the curve fit is unrestricted, there is some variation in the estimate for M_0. If defining the spread of the estimates as

$$S_r(M_0) \equiv \frac{\max(M_0) - \min(M_0)}{\min(M_0)} \cdot 100\%$$

which is the strictest way to define the spread of the estimated M_0, it is found that $S_r(M_0) \leq 10\%$ for each compound at each temperature, which indicates that there is no significant variation. Two exceptions are cyclohexane at 50 and 60 °C, which likely is due to convection, as increased temperature in the sample cell gives a larger temperature gradient over the sample. This sample is also the tallest, thus exposed to the largest temperature difference. At these temperatures, the difference between bottom and top of the sample has been estimated to 0.8 and 1.4 °C. As the viscosity is expected to follow an exponential form similar to the Arrhenius type equation, this is enough

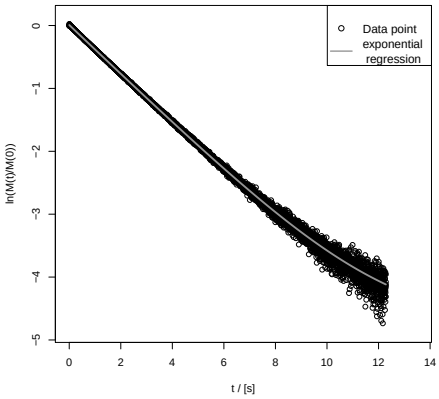

(a) Raw CPMG-data with the fitted 3-parameter model for $\tau = 1$ ms. The plot is semi-logarithmic.

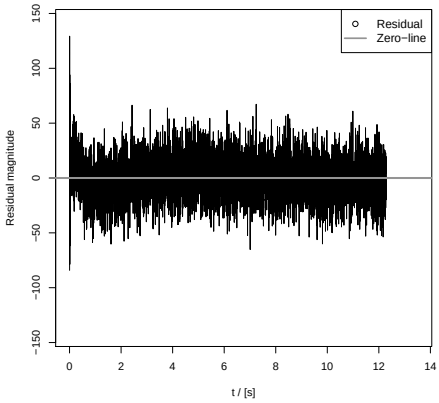

(b) Residual of CPMG-data fitted to the 3-parameter model for $\tau = 1$ ms.

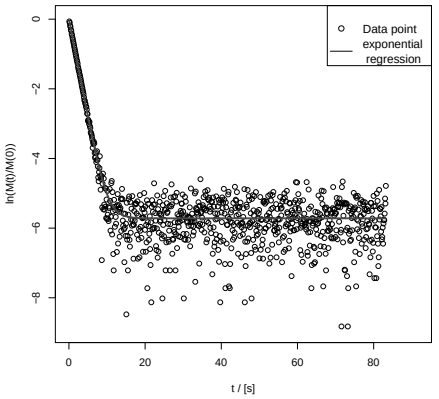

(c) Raw CPMG-data with the fitted 3-parameter model for $\tau = 52$ ms. The plot is semi-logarithmic.

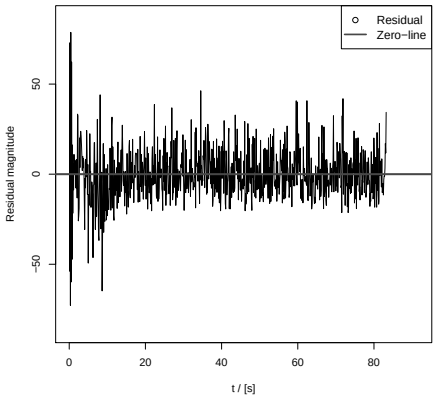

(d) Residual of CPMG-data fitted to the 3-parameter model for $\tau = 52$ ms.

Figure 5.4: Curve fits of raw CPMG-data with corresponding residuals.

to give a significant decrease in viscosity, leading to macroscopic flows that obscures the Brownian motion. The suspicion of convection is discussed in section 5.7 in terms of the estimated Rayleigh numbers.

The general trend for all systems is a decay in the estimated M_0, as can be expected as magnetization is lost in the first spin-echo when increasing τ, leading to a lower estimate for M_0. However, the estimated M_0 is not strictly decreasing, so for some systems the M_0 estimated at shortest τ is not the largest.

5.6.2 Systematic Error

The time parameters estimated for water shows some spiked peaks at $\tau_{\text{spike}} = 5,\ 15,\ 25,\ 35,\ 45$ ms, or with frequency $\nu = 100$ Hz. The raw data curves are presented in fig. 5.5, where the noise is clearly visible.

This noise proved repeatable for all temperatures and also for all samples investigated except for 1-pentanol, which has a modulating appearance. Therefore seems that some external or internal source interferes with the instrument, as it occurs at the same τ-values for all samples at all temperatures.

When inspecting the raw data, this noise manifests itself as "breaking" the signal curve, almost appearing as a discontinuity jump.

As four measurements were obtained at each value of τ, these were used to compute standard deviations s for each set. As it turns out, the standard deviations for the τ_{spikes}-values are several orders of magnitude larger than for the rest of the set of τ's, which supports the decision to neglect these measurements from further analysis.

Although no source has been identified, 100 Hz is known as a typical "refresh rate" in electronics as many electrical components sample or refresh at a frequency of 100 Hz, and is known to affect the measurements, [39]. The source might therefore prove difficult to pinpoint.

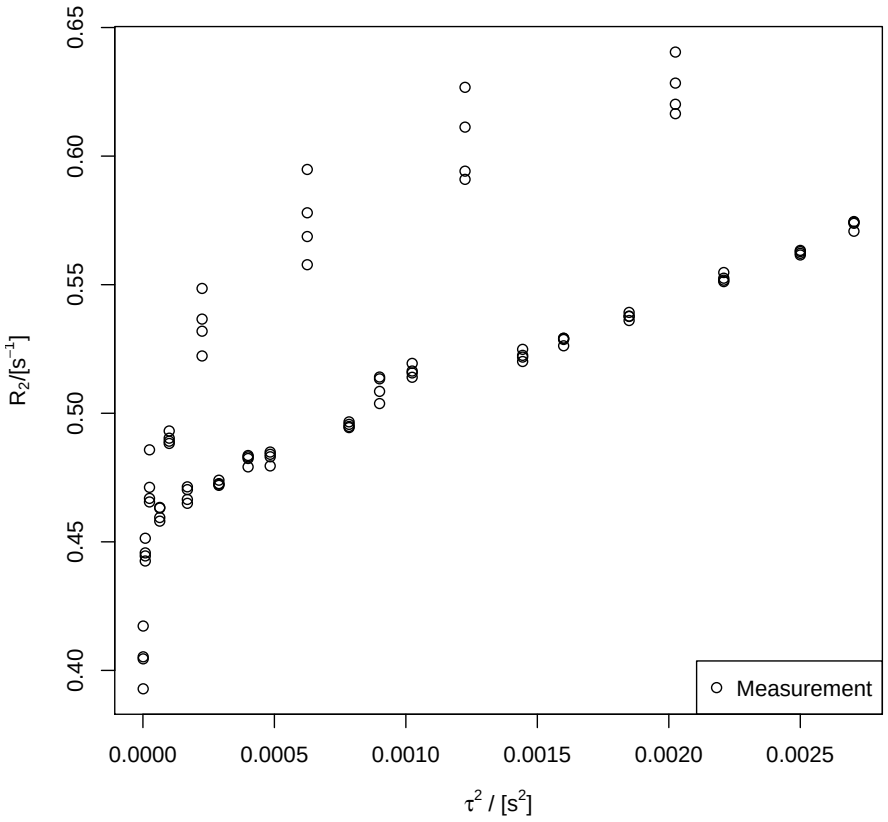

Figure 5.5: Apparent relaxation rate for water at 30 °C vs. τ^2.

5.6.3 T_2 from CPMG

Included in the CPMG-model is the term T_2, which is the transverse relaxation time. For simple liquids, theory dictates that $T_1 = T_2$ as long as the dominating mechanism is dipole-dipole coupling, [30]. Also, T_2 is sometimes estimated from a single CPMG-experiment with shortest possible value for τ. The compared estimates are given in table 5.7.

In this table, the third column from the right contains the mean values estimated by single CPMG curves for shortest possible τ, here $\tau_{\min} = 1$ ms. The right-most column contains the estimated values for T_2 estimated from eq. 2.35a.

In the case of 1-pentanol, the estimate is taken from eq. 2.25 on page 17 rather than eq. 2.35a. It can be seen from the uncertainties in the estimated values of T_2 that the model is highly unlikely, and it is most likely a coincidence that the model fits the observed data.

It should be noted that it is often found experimentally that $T_1 \neq T_2$. This is the case when other relaxation mechanisms than dipole-dipole coupling contributes, such as J-coupling, takes place [30].

The results obtained from the shortest curve and from linear regression are however not significantly different, so there is no need to perform a series of CPMG-experiments in order to estimate T_2, as long as a short enough τ is available.

Table 5.7: T_2 estimated by CPMG.

Compound	**Temp. / [°C]**	$\mathbf{T_2(\tau_{min})}$ **/ [s]**	$\mathbf{T_2}$ **/ [s]**
Benzene	30	9 ± 1	10.2 ± 0.2
Benzene	40	10.5 ± 0.2	11.45 ± 0.08
Benzene	50	11.0 ± 0.8	12.7 ± 0.1
Benzene	60	10 ± 2	14.3 ± 0.2
Cyclohexane	30	3.6 ± 0.2	3.65 ± 0.02
Cyclohexane	40	3.99 ± 0.08	4.09 ± 0.03
Cyclohexane	50	4.2 ± 0.4	4.71 ± 0.03
Cyclohexane	60	4.9 ± 0.2	5.37 ± 0.06
DMSO	30	2.61 ± 0.06	2.62 ± 0.02
DMSO	40	2.95 ± 0.05	3.02 ± 0.01
DMSO	50	3.28 ± 0.02	3.38 ± 0.01
DMSO	60	3.7 ± 0.2	3.76 ± 0.05
1-Pentanol	30	1.13 ± 0.02	2 ± 1
1-Pentanol	40	1.428 ± 0.005	3 ± 3
1-Pentanol	50	1.76 ± 0.02	5 ± 5
1-Pentanol	60	2.17 ± 0.01	6 ± 7
Water	30	2.47 ± 0.06	2.15 ± 0.01
Water	40	2.87 ± 0.01	2.56 ± 0.03
Water	50	3.1 ± 0.2	2.91 ± 0.02
Water	60	3.74 ± 0.08	3.67 ± 0.03

5.6.4 Estimates of the Squared Field Gradient

The goal of this thesis was to estimate the diffusion coefficient D by use of the inherent magnetic field inhomogeneities. As the diffusion coefficient is estimated from 2.35b, with B assumed to have a linear spatial dependency, the magnetic field inhomogeneities appear here as G_1^2, and it is simpler to estimate the magnetic field gradient squared than the gradient G_1, as the former may be estimated directly from the coefficients obtained by weighted linear regression. Both the squared gradient and the term $\frac{1}{3}D\gamma^2G_1^2$ is included in table 5.8. It appears that the uncertainties are independent of temperature and sample, as all relative uncertainties are of the same order of magnitude. The spread of the estimated values of $\frac{1}{3}D\gamma^2G_1^2$ is given in fig. 5.7. Here, the estimated slope of R_2^*, $\frac{1}{3}D\gamma^2G_1^2$, is plotted against literature values of D. The data points omitted from the sample space that were used to calculate the mean value are marked by solid coloring. An example of the weighted linear regression curve for R_2 vs. τ^2 is given in fig. 5.6 for water at 30 °C.

As the values estimated for cyclohexane at 50 and 60 °C and DMSO at 60 °C are significantly larger than the rest, these values are discarded. This is likely due to convection during the experiment, as seen from fig. 5.7 that these values are significantly larger than the rest.

Due to these reasons, the above mentioned results are exempted from the sample when calculating the sample mean. If the mean value $\bar{G}_1^2$ is compared to the median of the samples, $G_{1,\text{median}}^2 = 24 \cdot 10^{-6}$ T^2/m^2, the two estimates are within the uncertainty of $\bar{G}_1^2$. As the median is generally a more robust estimator than the mean, this supports the exclusion made earlier as the mean and median of the sample set are essentially equal [40].

Table 5.8: Estimated squared gradients, G_1^2. Starred compounds are omitted from the sample mean due to suspicion of convection.

Compound	**Temp / [°C]**	$\mathbf{\frac{1}{3}D\gamma^2G_1^2}$ **/ [s^{-3}]**	$\mathbf{G_1}^2$ **/ [10^{-6} T^2 m^{-2}]**
Benzene	30	46 ± 3	29 ± 2
Benzene	40	48 ± 2	26 ± 1
Benzene	50	50.8 ± 0.8	23.3 ± 0.4
Benzene	60	55 ± 1	21.8 ± 0.4
Cyclohexane	30	30 ± 1	28.2 ± 0.9
Cyclohexane	40	32 ± 1	25.8 ± 0.8
Cyclohexane*	50	47 ± 2	32 ± 1
Cyclohexane*	60	61 ± 2	36 ± 1
DMSO	30	13 ± 1	24 ± 2
DMSO	40	15.5 ± 0.9	24 ± 1
DMSO	50	17.1 ± 0.6	22.4 ± 0.8
DMSO*	60	30 ± 4	33 ± 1
Water	30	40 ± 2	24 ± 1
Water	40	56 ± 5	27 ± 2
Water	50	56 ± 2	22.3 ± 0.8
Water	60	61 ± 1	20 ± 1
Sample mean, $\bar{G}_1^2$	-	-	25 ± 3

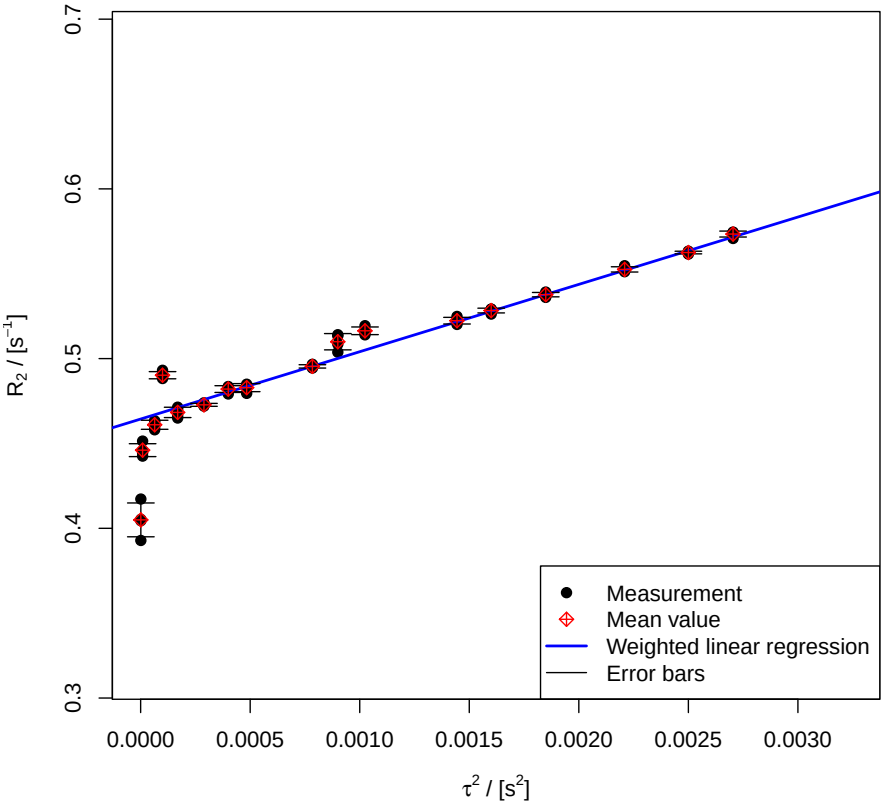

Figure 5.6: Apparent relaxation rate for water at 30 °C vs. τ^2.

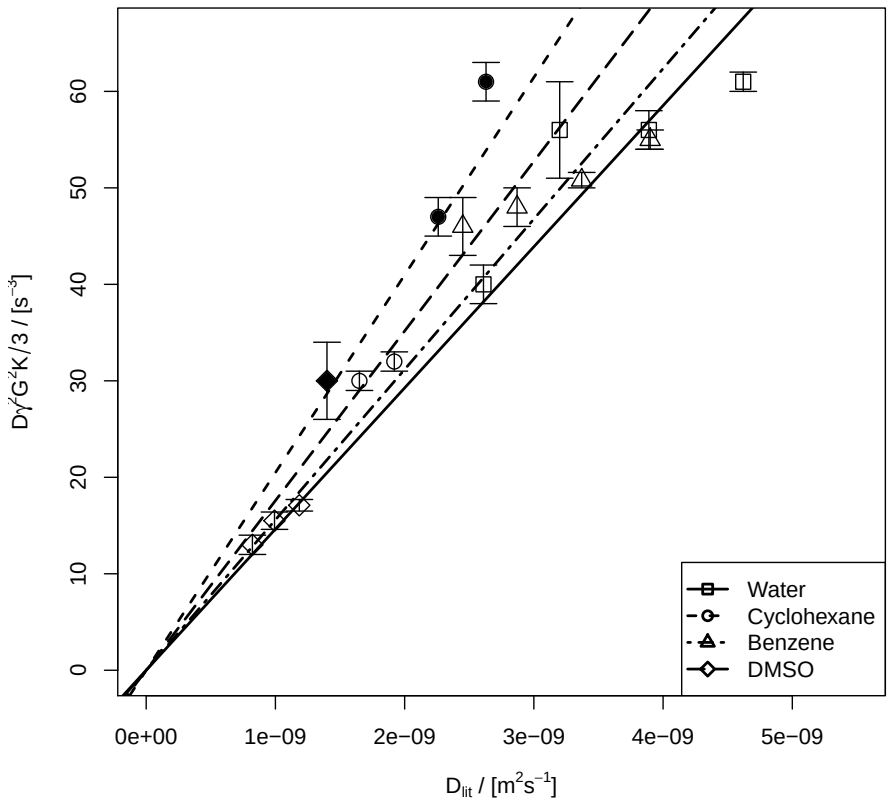

Figure 5.7: The estimated values for $\frac{1}{3}D\gamma^2G^2$ against literature values for D, listed in table 5.4 and 5.5 on page 49. Solid points are omitted from the sample mean as they appear to be overestimated.

5.6.5 Self-Diffusion Coefficients

By using the mean squared field gradient, $\bar{G}_1^2$, the diffusion coefficients D was estimated and are given in table 5.9. The difference is calculated relative to the literature values from [41, 25]. An illustration of the estimated self-diffusion coefficients are given in fig. 5.8, where a 90 % confidence interval has been added. The straight line in this figure, the "ideal line", is the line at which $D_{\text{exp}} = D_{\text{lit}}$.

The uncertainties in D are calculated from the uncertainty in the slope, $\frac{1}{3}D(\gamma G_1)^2$, of eq. 2.35b, and the uncertainty of $\bar{G}_1^2$ as

$$\delta D_{\max} = \max\left\{\frac{3\left(B \pm \delta B\right)}{\gamma^2\left(\bar{G}_1^2 \mp \delta\bar{G}_1^2\right)}\right\}$$

where $B = \frac{1}{3}D\gamma^2 G_1^2$ is the estimated slope and δB is the corresponding standard deviation of B, both listed in table 5.8.

Table 5.9: Diffusion coefficients D estimated by use of the mean squared gradient, $\bar{G}_1^2$. The diffusion coefficients for DMSO are the same as those given in table 5.5.

Compound	**Temp / [°C]**	**D_{lit} / [10^{-9}m^{2}s^{-1}]**	**D / [10^{-9}m^{2}s^{-1}]**	**Difference / [%]**
Benzene	30	2.45 ± 0.03	3 ± 1	22
Benzene	40	2.87 ± 0.03	3.0 ± 0.9	4.5
Benzene	50	3.37 ± 0.07	3.2 ± 0.7	5.0
Benzene	60	3.90 ± 0.08	3.47 ± 0.5	12
Cyclohexane	30	1.65 ± 0.01	2 ± 2	21
Cyclohexane	40	1.92 ± 0.04	2 ± 1	4.2
Cyclohexane	50	2.26 ± 0.04	3 ± 1	33
Cyclohexane	60	2.63 ± 0.07	3.9 ± 0.5	48
DMSO	30	0.82 ± 0.03	0.82 ± 0.06	0
DMSO	40	0.99 ± 0.03	0.98 ± 0.06	1.0
DMSO	50	1.19 ± 0.04	1.08 ± 0.04	9.2
DMSO	60	1.40 ± 0.04	1.9 ± 0.3	36
Water	30	2.61 ± 0.1	3 ± 2	15
Water	40	3.20 ± 0.04	3.5 ± 0.8	9.4
Water	50	3.89 ± 0.06	3.5 ± 0.8	10
Water	60	4.62 ± 0.03	3.85 ± 0.05	17

It is difficult to explain the large difference for benzene at 30 °C, but all other estimates are reasonable when compared to literature values. The exceptions here are DMSO and cyclohexane at 60 °C and also cyclohexane at 50 °C. However, these samples have the largest Rayleigh numbers, estimated in section 5.7, which supports convection as an explanation. Although the estimated Rayleigh numbers from section 5.7 indicates convection in all samples except water at the lowest temperature, the reasonably good fit between the literature values of the diffusion coefficient and the estimate made by use of estimated $\bar{G}_1^2$ indicates that the Rayleigh numbers estimated are not very good. There may be two explanations; either better estimates of the parameters α, ν, κ are needed, or the sample tube is too narrow to allow for Bénard cells, suppressing the convection.

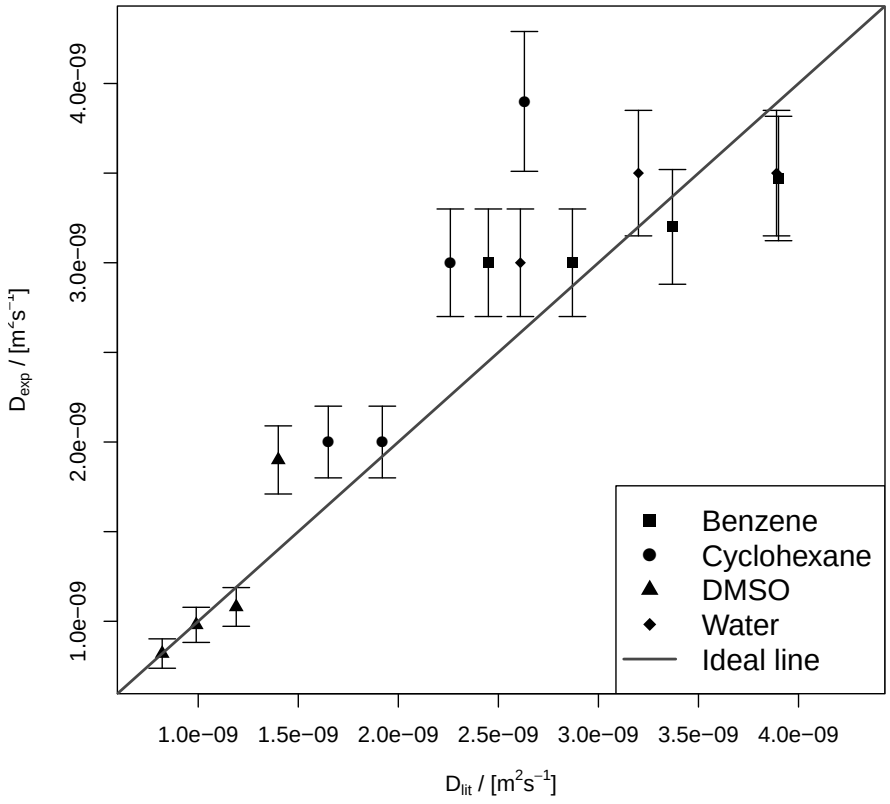

Figure 5.8: The self-diffusion coefficients estimated by us of CPMG vs. literature values. The straight line is the line at which $D_{\text{exp}} = D_{\text{lit}}$. The bars denotes 90 % confidence intervals.

5.6.6 1-Pentanol

The CPMG results for 1-pentanol showed a modulating form, as shown in fig. 5.9 and is in accordance with eq. 2.25 on page 17. Hence, systems with strong J-coupling needs a different approach when analyzed.

Interestingly, the J-coupling constant for 1-pentanol should be possible to estimate from eq. 2.25, and the estimates are listed in table 5.10. If comparing these values to those listed in [31], these estimations points to CH-coupling in 1-pentanol as the dominating effect.

As only about 1 % of naturally occurring carbon nuclei are NMR-active, it is unlikely to observe this strong coupling from J-coupling between a carbon and a proton. Typical values for J-coupling between hydrogen are listed in [31] as 276 Hz in H_2 and 0-30 Hz for protons with one intervening bond.

Thus, the good fit of eq. 2.25 to the estimated R_2 appear to be a mere coincidence.

Table 5.10: Estimated values for the J-coupling constant.

Temperature / [°C]	$\mathbf{\Delta_\infty}$ **/ [s^{-1}]**	**J / [s^{-1}]**
30	6.4 ± 0.3	147 ± 3
40	6.3 ± 0.3	144 ± 4
50	6.2 ± 0.3	141 ± 3
60	6.0 ± 0.2	140 ± 3

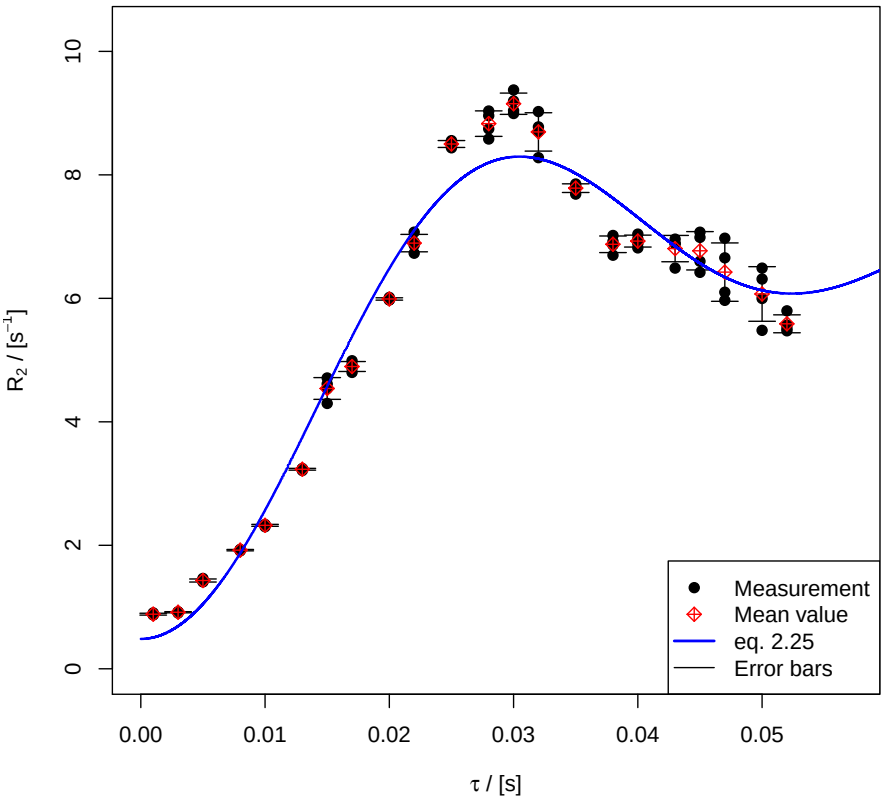

Figure 5.9: Apparent relaxation rate for 1-pentanol at 30 °C vs. τ.

5.6.7 Tetrahydrofuran

The CPMG response of THF was obtained to see how a system with different chemical shifts would behave in this experiment. As previous experiments indicated that the diffusion is detectable, and therefore could be expected to yield good results, diffusion measurements by CPMG of THF were performed.

The problem with the obtained curves is that the two signal sources are impossible to separate under the current conditions, leading to a signal likely superposed by the CPMG-signal from one proton and the observed oscillation from an off-resonance proton. This assumes that the instruments automated function for determining on-resonance manages to lock on to one of the protons, and always the same proton. If this assumption is wrong, then the process of separating the signals becomes even more complex.

The normalized signal should now take the form of a bi-exponential,

$$\hat{M}(t) = p_1 e^{-t/T_{2,1}} + p_2 e^{-t/T_{2,2}} \tag{5.7}$$

with p_i being the proportion of the retrieved signal from the i-th proton and $T_{2,i}$ being the transverse relaxation time for the i-th proton. The four protons of THF belongs, according to symmetry, to two different chemical shifts, and it is these two shifts that gives rise to the two exponentials in the expression.

The data from one CPMG-experiment with $\tau = 0.022$ s is displayed in fig. 5.10. As the plot is log-linear, it is seems that the data are single-exponential, and the data set could be fitted to a single exponential although this obviously is wrong.

As neither `R` 's `nls()`-package nor commercial software (WinFit) managed to fit eq. 5.7 to all the CPMG-signals, and the single-exponential expression is obviously wrong, all further analysis of the THF-data was abandoned.

The data set still serves some use, as it demonstrates a system too complex for measuring the diffusion coefficient by the approach used in this work.

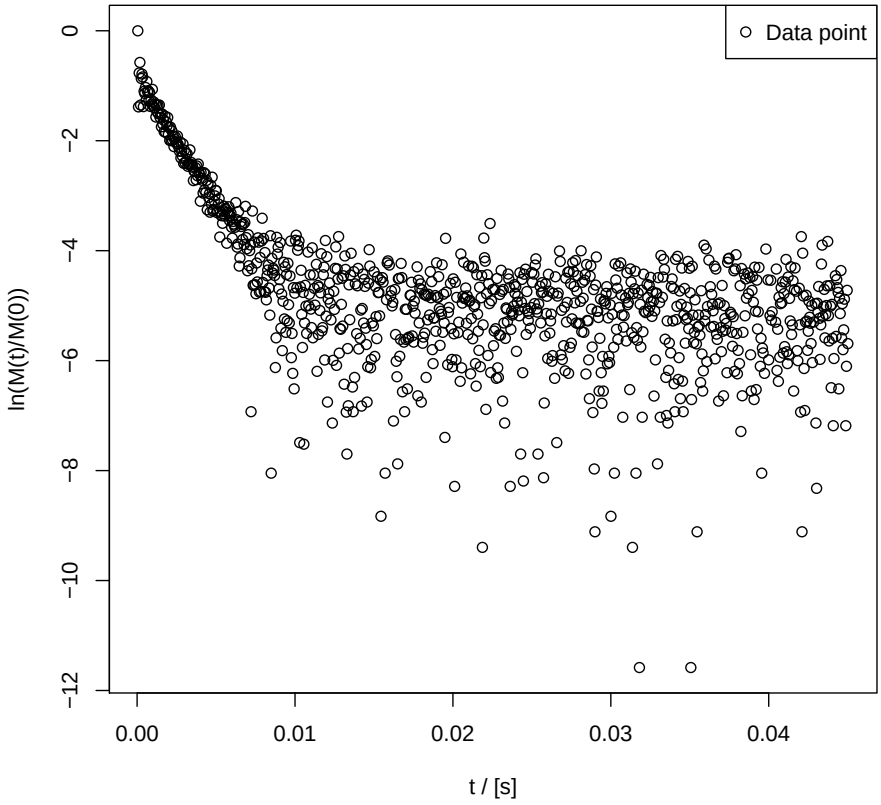

Figure 5.10: Raw CPMG data for THF at 30 °C. $\tau = 0.022$ s. The plot is semi-logarithmic.

5.6.8 Sensitivity of R_2 to Self-Diffusion

Except for 1-pentanol and THF, the transverse relaxation curves of all systems could be approximated by eq. 2.35b. Depending on the value of G_1^2, which is assumed to be a "fixed" magnetic field parameter, there is an issue with the magnitude of the diffusion coefficient, as a compound with sufficiently low diffusion coefficient is not traceable.

The borderline sensitivity of the diffusion can be estimated from the same model used to estimate the gradient squared, by fixing G_1^2 to the value estimated in section 5.6.5. If allowing for a 90 % confidence interval, a representative estimate of the uncertainty in the estimate of G_1^2, the diffusion coefficient D appears to be possible to extract down to $1 \cdot 10^{-11}$ m^2 s^{-1}. For systems with a smaller diffusion coefficient, the estimation might be attainable for larger values of τ, but as an increasing τ gives a smaller number of points defining the decaying magnetization, this approach gives a less reliable characterization of the relaxation curve. The various estimates are given in fig. 5.11, where the contributions from diffusion in an inhomogeneous magnetic field has been calculated for various values of the diffusion coefficient. From these results, it appears that the smallest self-diffusion coefficient that can be determined is in the order of $1 \cdot 10^{-11}$ m^2 s^{-1}.

Some of the R_2-curves shows a "dip" at short R_2. This is likely due to the local magnetic field having a more complex form than the assumed linear form. This means that for short values of τ, the molecules will not have traveled very far, thus experienced a smaller part of the magnetic field. For $\tau = 1$ ms, the rms-distance for a 3-dimensional random walking water molecule at 30 °C is estimated to be $r_{\text{rms}} = \sqrt{6D\tau} \approx 4$ μm, whereas for $\tau = 52$ ms, $r_{\text{rms}} \approx 30$ μm, seven times as far. This indicates that when τ gets sufficiently long, the molecules experiences more of the magnetic field inhomogeneities and the relaxation due to magnetic field inhomogeneities becomes more prominent. Therefore, it seems necessary to ensure that CPMG-experiments with sufficiently long τ are used, as curves obtained for short τ will not capture the averaged magnetic field inhomogeneities. In general, the $R_2(\tau)$ has a τ^2-dependency, as shown earlier, whereas the rms-distance has a $\sqrt{\tau}$-dependency. As R_2 has an implicit dependency of r_{rms}^4, it is therefore possible to observe this effect at short τ. This indicates that the local gradients are much larger than the estimated G_1, which is the sample average. If applying a magnetic field gradient of the strength estimated in this work, diffusion measurements would not prove successful. However, as the local magnetic inhomogeneities are much larger, diffusion still proves detectable

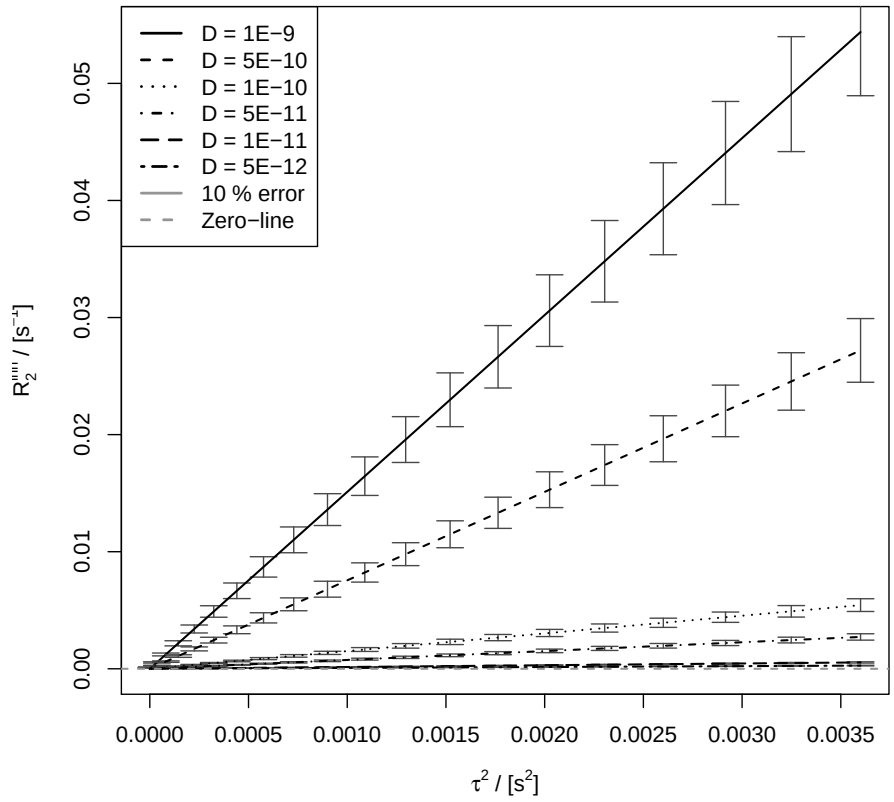

Figure 5.11: Simulated relaxation rate for various diffusion coefficients.

and the diffusion coefficient can be measured.

5.6.9 Activation Energies of the Self-Diffusion Process

The activation energies for the diffusion coefficients D were estimated by weighted nonlinear regression from the equation

$$B = B_0 e^{-\Delta E/RT} \tag{5.8}$$

with $B = \frac{1}{3}\gamma^2 G^2$. As $B \propto D$, the estimated activation energy should be the same as for the Arrhenius-type equation, eq. 2.11. Although it is noted that water has non-Arrhenius behavior, [25], it might be approximated as such for the temperature range investigated within this thesis. Although the Speedy-Angel-power law, reviewed in [25], accounts for interesting behavior of supercooled water, it is irrelevant in this context. The activation energies estimated from B are listed in table 5.11 together with the activation energy estimated from the literature values of the diffusion coefficient, denoted ΔE_{lit}. The differences are relative to the estimates made from literature values of D.

As four data points are quite few for estimating the parameters, the uncertainties becomes quite large when some data points are flawed. In this case, flawed data are diffusion coefficients estimated for samples with convection. The bad estimate for benzene may stem from the apparent over-estimation of the diffusion coefficient at 30 °C. For cyclohexane, the estimated diffusion coefficients and the analysis of the Rayleigh number indicated quite strongly that convection could be a problem. The estimated activation energies for water and DMSO does not fit well with those estimated from literature values either. Due to the large standard deviations in the activation energies estimated from the slope B, the estimate for DMSO is within one standard deviation of the estimate made from literature values of D. The estimates for cyclohexane are within two standard deviations of each other, and the estimate for water within three. The estimates made for benzene are the only that are significantly different. The standard deviations referred to are those of ΔE estimated from B.

Table 5.11: Estimated activation energies from CPMG-measurements.

Compound	**ΔE/ [kJ mol^{-1}]**	**ΔE_{lit}/ [kJ mol^{-1}]**	**Difference / [%]**
Benzene	5.8 ± 0.8	13.0 ± 0.2	55
Cyclohexane	22 ± 5	12.8 ± 0.2	72
DMSO	12 ± 6	14.87 ± 0.09	19
Water	10 ± 2	15.9 ± 0.2	37

5.6.10 The Shape of the Magnetic Field Inhomogeneities

An expression for the relaxation time has been derived for CPMG- and Hahn echo-experiments, assuming a second-order polynomial form of the magnetic field $B = B(0) + G_1 z + G_2 z^2$. The ratio $k = G_2/G_1$ has been estimated to $k = -88.4 \pm 0.2$ m^{-1} in [19] from the apparent relaxation rates of benzene, cyclohexane and water. Scaled to 1 cm, a typical sample height for the sample used, this gives that the second-order term is $\approx 88\%$ of the first-order term pr. cm. The parameter k was estimated by fitting eq. 2.36 simultaneously to all apparent relaxation curves and assuming that G_1^2 is the same for all samples, and modelling the correction faktor $K(k, L, \rho, \ell)$ by inserting the values for L and ρ for each sample and assuming $\ell = 0$.

The form of the magnetic field inhomogeneities is illustrated in fig. 5.12 together with the linear model, and it can be seen from this figure that the second-order field approximation gives the form of an inverted parabola over the range of 1 cm. It can be seen the derived model, eq. 2.36, that the model inflicts the CPMG-signal if the parameters L, ℓ, ρ are changed during experiments. Especially, the second-order polynomial implies that the term $B(0)$ cannot be set to zero due to gauge invariance when if the vertical position of the sample is changed, as can be done for a linear model.

5.6.11 The Shape of the K-function

As it has been shown that the magnetic field inhomogeneities have a second-order form in z, the sensitivity to the parameters ℓ, ρ and L is of importance to the NMR signal, as the correction factor $K(k \neq 0, L, \ell, \rho) \neq 0$.

Defining the relative change in the K-function as

$$\Delta K(k, L, \ell, \rho) = \frac{K(k, L, \ell, \rho) - K(0.884, 1, 0, 0.5)}{K(0.884, 1, 0, 0.5)}$$

where all lengths are given in cm and the variables of the reference function are fixed to $k = -0.884$ cm^{-1}, that is the value estimated in [19], with the sample height fixed to $L = 1$ cm. The vertical displacement was ignored, $\ell = 0$ cm and the ratio ρ was fixed as $\rho = 0.5$.

From the figures produced, fig. 5.13, it can be seen that the parameters affects the correction function in various ways. Although the dependency of L, ℓ, ρ can be seen from the derived expression for K, they will be discussed as they may not manifest themselves as such. For example, a quadratic function will over a sufficiently short range appear as linear, and therefore the apparent forms will be commented on.

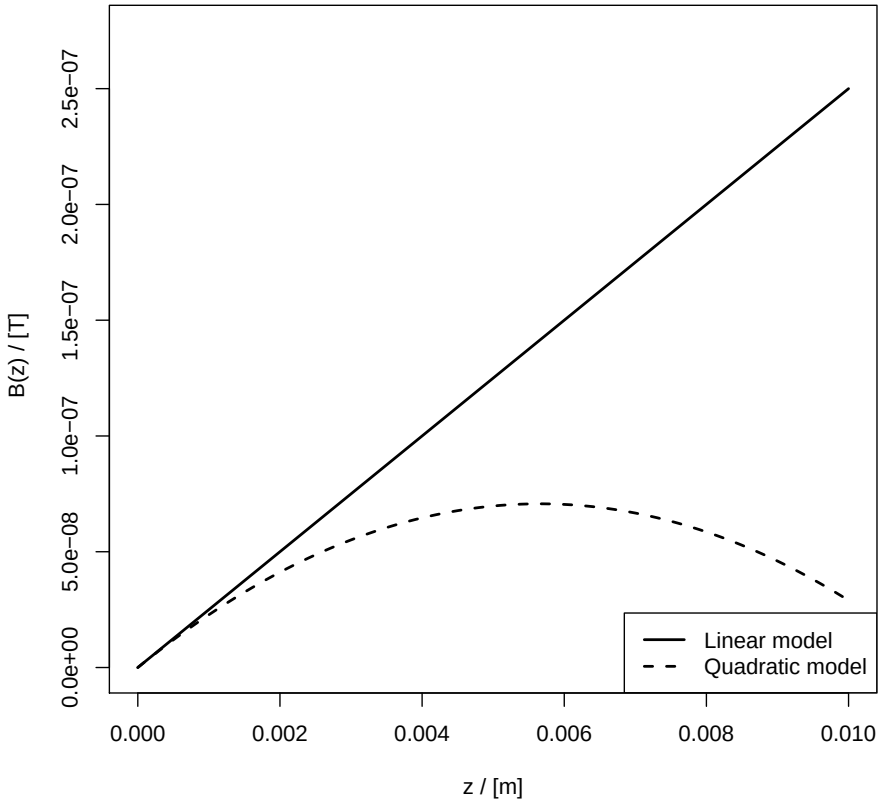

Figure 5.12: The linear and quadratic model for the magnetic field inhomogeneities over a range of 1 cm.

Starting with fig. 5.13a, the effect of L appears as weakly quadratic for a sample height ranging from zero to two cm. As the height of the sample affects the effect of the curvature of the magnetic field gradient, this affects the K-function the strongest.

From fig. 5.13b, the effect of ρ clearly seems to be a cubic relationship over a range from zero to two cm. Increasing ρ leads to a smaller value for K, as an increasing ρ simulates a wider tube. As L is held fixed, this does not account for a decreasing sample height and only signifies that the larger the hemisphere, the less the value for K becomes, as the "limit" for increasing ρ gives the geometry for a NMR-tube in the shape of a hemisphere.

Lastly, in fig. 5.13c, the effect of ℓ is clearly a linear effect, and nothing else is to be expected from the expression for K. The effect of ℓ is in between that of L and ρ in magnitude, but due to the linear dependency, removing and re-inserting a sample into the sample cell may lead to difficulties interpreting the signal. As long as ℓ is not intended to change, this might be countered by ensuring that the sample tubes are not removed during a long experiment, and preferably use a sample position gauge device for determining the sample position reproducibly.

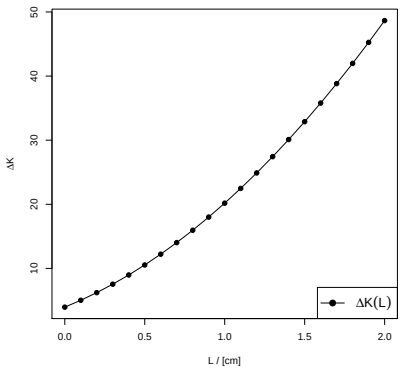

(a) The effect of L on the correction function K.

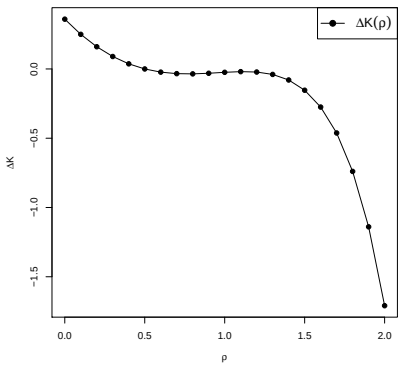

(b) The effect of ρ on the correction function K.

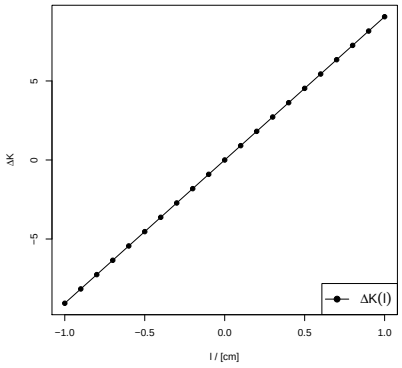

(c) The effect of ℓ on the correction function K.

Figure 5.13: The effect of the parameters L, ℓ and ρ on the correction function $K(k, L, \ell, \rho)$.

5.7 Convection

5.7.1 Qualitative Outline

The best way to analyze convection is usually in terms of the Rayleigh number, Ra. As the Rayleigh number is dependent on a set of sample parameters α, ν and κ, the Rayleigh number may not be calculated without values for these parameters. As only DMSO, benzene, cyclohexane and water is considered in this discussion, a simplification may be made by assuming that all parameters are of the same order of magnitude. As the Rayleigh number is usually discussed in terms of order of magnitude, this assumption can be used to describe the problem qualitatively.

The Rayleigh number has two variables, the characteristic temperature difference scale Θ and characteristic length scale L. Here, L is the sample height and Θ is the temperature difference between the bottom of the sample and the top of the sample. For simplicity, it is assumed that the bottom of the sample is the same in all cases and that the only difference between the samples is the total temperature difference over the sample due to varying sample height.

If assuming a linear, one dimensional, temperature gradient, $\nabla T = \partial T/\partial z = \Delta T/1$ cm, Θ can be rewritten as $\Theta = \partial T/\partial z \cdot L$ as the temperature difference ΔT has been estimated over a range of 1 cm. The estimated temperature differences are listed in table 4.3. This rewriting allows Θ to depend on sample height, and the Rayleigh number given in eq. 2.14 may be rewritten as

$$\mathrm{Ra} = \mathrm{Pr} \cdot \mathrm{Gr} = \frac{g\alpha\Theta L^3}{\nu\kappa} = \frac{g\alpha\frac{\partial T}{\partial z}L^4}{\nu\kappa} \tag{5.9}$$

As $\partial T/\partial z$ is considered fixed at each temperature setting, the Rayleigh number now only depends on sample height, giving the Rayleigh number an implicit dependency of L^4.

If now introducing a scaled Rayleigh number as

$$\mathrm{Ra}' = \frac{\mathrm{Ra}\nu\kappa}{g\alpha\frac{\partial T}{\partial z}} = L^4 \tag{5.10}$$

the variation in Rayleigh numbers might be seen by comparing the tallest sample, cyclohexane, to the second-to-closest one, that is water or DMSO. This only makes sense as long as the assumption that the parameters α, ν, κ are of the same order of magnitude holds.

The effect of sample height on the scaled Rayleigh numbers might be estimated by comparing the tallest and second to tallest sample,

$$\frac{\mathrm{Ra}'_{\mathrm{Cyclohexane}} - \mathrm{Ra}'_{\mathrm{Water}}}{\mathrm{Ra}'_{\mathrm{Water}}} = \frac{L^4_{\mathrm{Cyclohexane}} - L^4_{\mathrm{Water}}}{L^4_{\mathrm{Water}}} = \frac{1 - 0.8^4}{0.8^4} = 1.44$$

so a difference in L of 2 mm gives a 144 % increase in the scaled Rayleigh number. If comparing the tallest sample, cyclohexane, to the shortest of sample, benzene, the scaled Rayleigh numbers is 216 % larger, and this sample is just 1 mm shorter than those of water and DMSO. If the assumption that the sample parameters are of the same order of magnitude, this difference will be transferred to the Rayleigh number.

The difference between benzene and DMSO/water (the shortest sample and the two middle), is 29 % in terms of the scaled Rayleigh number.

From this simplified analysis, it seems clear that the cyclohexane sample is most exposed to convection as it clearly has the largest scaled Rayleigh number.

5.7.2 Estimated Rayleigh Numbers

As there exist some estimates of α, ν and κ, the Rayleigh number for each sample at each temperature may be estimated. The temperature differences from table 4.3 will be used together with the form of the Rayleigh number in eq. 5.10 to approximate the temperature difference Θ as a linear gradient, $\Theta = \frac{\partial T}{\partial z} \cdot L$. As it does not matter in which direction the convection is, the temperature difference at 30 °C is listed as the absolute value. The parameter values with corresponding Rayleigh number are listed in table 5.12. An illustration of the estimates are given in fig. 5.14, where it can be seen that the estimated Rayleigh numbers for cyclohexane are indeed very much larger than the others.

The parameters listed in table 5.12 are taken from several sources. Published estimates of the thermal diffusivity coefficient, κ, could not be found for any of the compounds used except for water at 20 °C, and this value of κ have been used for all samples as an approximation, [27]. Although the various parameters are taken to vary weakly with temperature, all other coefficients have been listed only to the first digit as the deficiency in data for κ limits the certainty of the Rayleigh number.

The kinematic viscosity for DMSO have been calculated from the relation $\nu = \mu/\rho$, that is, the dynamic viscosity over the mass density. The dynamic viscosity and specific gravity of DMSO, relative to that of water, was found in [42].

The parameter values for benzene and cyclohexane were found at the web page of the Dortmund Data Bank, `http://www.ddbst.com/en/EED/Explorer%20Edition%20Data.php`, and all references are taken from this webpage. As the kinematic viscosity is dependent on pressure, the values estimated at 100 kPa where used when available. Although the pressure in the NMR tubes have not been determined exactly, the relative pressure may increase by 10 % if the vapour in each tube is approximated as an ideal gas. This increased pressure is however ignored for now.

The kinematic viscosity of benzene at 30° were taken from [43] and at 50° from [44]. The values at 40 and 60 °C was estimated from the mean of [43] and [44], and [44] and [45] respectively. The thermal expansion coefficients of benzene were all found in [46].

The kinematic viscosity of cyclohexane at 30 and 60 °C were taken from [47] and [48] respectively. The kinematic viscosity at 40 and 50 °C were interpolated by linear regression using the estimates for 30 and 60 °C as the the kinematic viscosity has a linear increase at this temperature range. The thermal expansion coefficients of cyclohexane were all found in [49]. Although the coefficients were estimated at 5 times as high pressure as used in this work, it is the best estimate available..

For water, all parameters were used as listed in [27]. Although these estimates are all at atmospheric pressure and 20 °C, they are the best estimates available for water. At the web page of the Dortmund Data Bank, the only available data were kinematic viscosity coefficients at 22 MPa, and these are not useful here.

As many of the Rayleigh numbers estimated are larger than the critical Rayleigh number at 1078, this indicates almost every sample is likely to have convection at all temperatures except water at 30 °C. As the results in section 5.6.5 are mostly in line with estimates from the literature, it seems that better estimates of the parameters α, ν, κ are needed in order to estimate precise enough Rayleigh numbers.

Table 5.12: Estimated Rayleigh numbers for each sample at each temperature. The references for the various parameters are given in section 5.7.2.

Compound	**Temperature difference / [K]**	$\boldsymbol{\alpha}$ / $[10^{-3}$ **K**$^{-1}]$	$\boldsymbol{\nu}$ / $[10^{-6}$ **ms**$^{-2}]$	$\boldsymbol{\kappa}$ / $[10^{-7}$ **ms**$^{-2}]$	**Ra** / $[\mathbf{10^3}]$
Benzene	0.3	1	0.7	2	5
Benzene	0.4	1	0.6	2	8
Benzene	0.8	1	0.5	2	20
Benzene	1.4	1	0.5	2	30
Cyclohexane	0.3	1	1	2	10
Cyclohexane	0.4	0.9	1	2	20
Cyclohexane	0.8	0.8	0.8	2	40
Cyclohexane	1.4	0.7	0.7	2	70
DMSO	0.3	0.9	2	2	3
DMSO	0.4	0.9	2	2	4
DMSO	0.8	0.9	1	2	10
DMSO	1.4	0.9	1	2	30
Water	0.3	0.2	1	2	1
Water	0.4	0.2	1	2	2
Water	0.8	0.2	1	2	3
Water	1.4	0.2	1	2	6

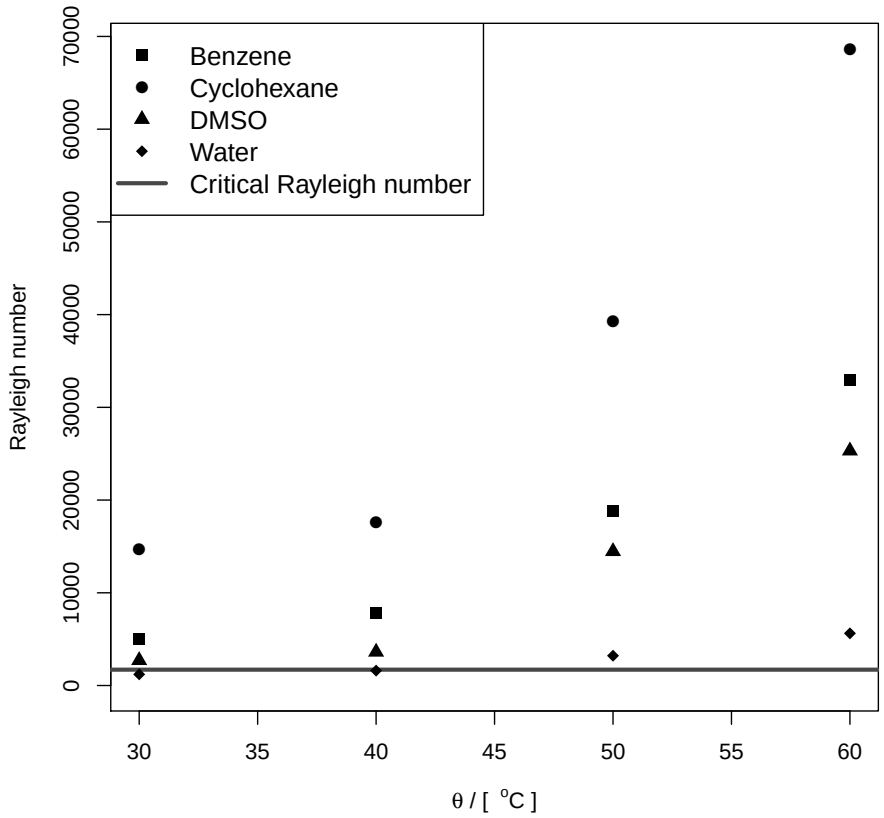

Figure 5.14: A visual comparison of the estimated Rayleigh numbers vs. temperatures used experimentally.

Chapter 6

Conclusions

6.1 The Form of the Magnetic Field Inhomogeneities

The principal findings of this thesis is that the magnetic field inhomogeneities of the instrument used are sufficient for probing diffusion by use of CPMG-experiments, as tested by use of six different sample molecules. The magnetic field inhomogeneities may be approximated by a linear, squared magnetic field gradient, estimated to 25 $\mu\mathrm{T}^2$ m^{-2}. By generalizing the equations for the CPMG-signal, it has been shown that the field is better described by a quadratic spatial dependency by introducing a correction function K dependent on the magnetic fields curvature, G_2, the total sample height, L, the vertical displacement of the sample, ℓ, and the radius of the hemisphere of the NMR tubes, r_0. The magnetic field curvature G_2 has been discussed in terms of the ratio $k = G_1/G_2$, and the effect of the radius of the tube in terms of the ratio between the radius r_0 and the total sample height L, $\rho = r_0/L$. This discussion demonstrated that the linear approximation may not be suitable for large variations of L, ℓ, ρ. As these variations affect the measurements, they may be compensated for by using the correction function K. From [19], the value of k has been estimated to $k = -88.4$ m^{-1}. For samples with sufficiently short sample height, the linear approximation becomes more valid. A shorter sample height also helps minimize convection due to temperature gradients in the sample cell. In the linear approximation, the Hahn echo was found to give an estimate of the magnetic field gradient consistent with the estimation by CPMG, when correcting for a factor of four that arises from the different diffusion times in the two experiments.

6.2 Estimation of Diffusion Coefficients and Activation Energies

From the linear approximation and by use of literature values as reference values, the diffusion coefficients for four of the six sample molecules used have been estimated, in most cases within 10-20 % of the literature values. The activation energy of the the Arrhenius-type equation have been estimated from the slope of the apparent relaxation rates. The application of diffusion measurements by CPMG have been demonstrated as limited to molecules where the dominating relaxation mechanism is the dipole-dipole coupling and all protons are in a chemically equivalent environment, as demonstrated from the experiments with 1-pentanol and THF. A sensitivity analysis, using the estimated squared magnetic field gradient for the linear model, have been made, indicating that the lower limit for detectable diffusion coefficients are in the order of 10^{-11} m^2 s^{-1}.

6.3 Estimation of Transverse Relaxation times

The use of single CPMG-curves to estimate the transverse relaxation times has been verified to be sufficient even in an inhomogeneous magnetic field by comparing the transverse relaxation times estimated from a single CPMG-curve to the value estimated be weighted linear regression for a series of CPMG-experiments with increasing inter-pulse time. The only condition seems to be that the inter-pulse time can be made sufficiently short. The shortest inter-pulse time used in this work has been 1 ms.

It has also been demonstrated that the FID should not be used to estimate the transverse relaxation rate in the presence of magnetic field inhomogeneities, as the magnetic field inhomogeneities affects the decay of the signal so that it can no longer be approximated by a single, decaying exponential.

6.4 The Presence of Convection

As several of the samples tested have given diffusion coefficients significantly different from literature values, the effect of convection has been discussed. From the values of the parameters α, ν, κ obtained, the corresponding Rayleigh number has been estimated. As almost all Rayleigh numbers estimated exceeds the critical Rayleigh number, convection may be present in all these samples. The only exception seems to be water at 30 °C. However, as some of the parameters used to estimate the Rayleigh numbers have been for

different molecules or at different states than those used here, these estimates are not reliable. The true Rayleigh numbers may therefore be calculated to be much smaller if the parameter estimated for the correct molecule at the correct state were used to estimate the Rayleigh numbers. Also, the sample tube may be too narrow for Bénard flow to establish itself so that the sample tube suppresses the convection. If the latter is true, then the Grashof number used to calculate the Rayleigh number has the wrong form, and a different form should be used. This may have to be derived, as the NMR tube represents a geometry for the problem somewhat different from the classical examples in fluid mechanics.

6.5 Future Work

- The samples should be remade, using cylindrical tubes for all samples and have an equal sample height in order to redo the measurements and validate the estimates made in this thesis.
- Applying the outlined method to a system compromised mainly of similar protons, such as polymers or polymer solutions.
- For the discussion of convection, better estimates are needed for the thermal expansion coefficient, the kinematic viscosity and the thermal diffusivity coefficient as some of the approximated values used here are very crude. This may be obtained by searching the literature further, or by obtaining them experimentally.
- Methods for minimizing the temperature gradient over the sample cell should be investigated. Right now, the simplest solution is to prepare samples with a smaller amount of liquid.
- Applying the method to a high-field instrument, using the shimming magnets to make the magnetic field intentionally inhomogeneous.

Appendix A

Calculating an Even-Spaced τ-List for the Inversion Recovery–Experiments

In order to estimate the parameter T_1 for a sample, it is necessary to perform a form of recovery-experiment at different time interval,s τ, after relaxation has begun.

This appendix shows how to calculate these values for an inversion recovery—experiment in order to obtain evenly spaced magnetism. A sketch of the idea is given in fig. A.1 on the next page, where the goal is to get the black horizontal lines evenly spaced.

The results from section A.1 are then presented as a numerical implementation in section A.2.

A.1 Determining τ-values from a Recursion Relationship

For a single spin-system, it is well known, from solving eq. 2.19 on page 13 with appropriate boundary conditions, that the spin-lattice relaxation behaves as

$$\frac{M(\tau)}{M(0)} = \hat{M}(\tau) = 1 - 2e^{-\tau/T_1} \tag{A.1}$$

with the boundary conditions being

$$\hat{M}(0) = -1 \quad \text{and} \quad \hat{M}(\tau \to \infty) = 1.$$

The intensity spacing between two consecutive measurements then be-

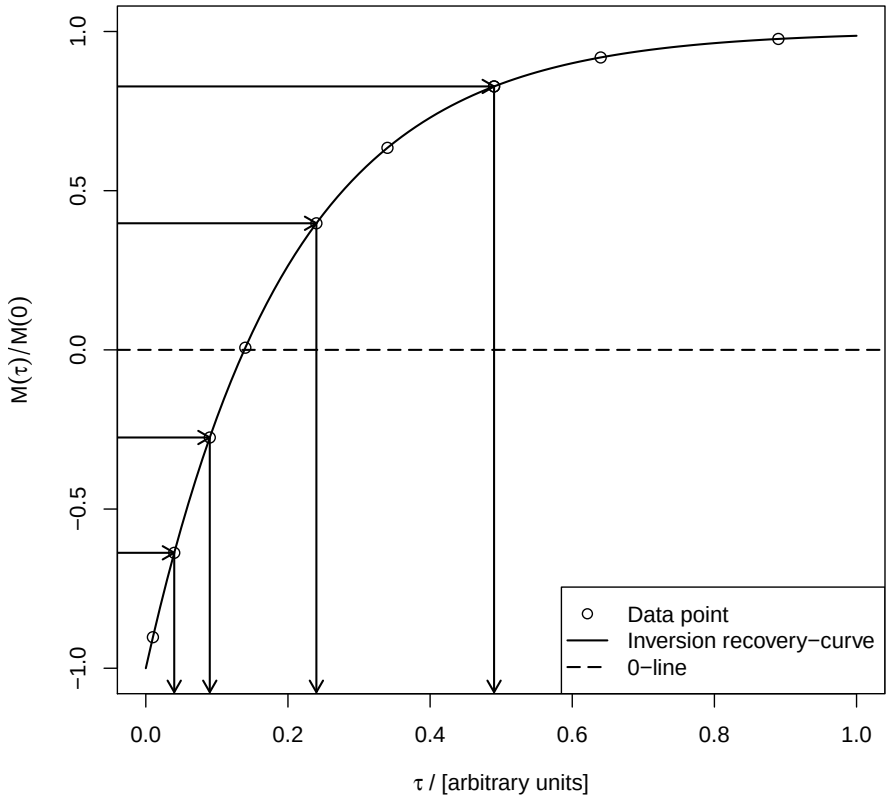

Figure A.1: A sketch of the ideal spacing of magnetization in an inversion recovery–experiment and corresponding τ-values for experimental use.

comes

$$\hat{M}_{i+1} - \hat{M}_i = \frac{\hat{M}(\tau \to \infty) - \hat{M}(0)}{N} = \frac{2}{N} \tag{A.2}$$

with $\hat{M}_i$ being the magnetization at time τ_i and N being the number of τ-values.

Substituting eq. A.1 into eq. A.2 yields

$$\begin{aligned}\left(1 - 2e^{-\tau_{i+1}/T_1}\right) - \left(1 - 2e^{-\tau_i/T_1}\right) =& \frac{2}{N} \\ e^{-\tau_i/T_1} - e^{-\tau_{i+1}/T_1} =& \frac{1}{N} \\ e^{-\tau_{i+1}/T_1} = e^{-\tau_i/T_1} -& \frac{1}{N}\end{aligned}$$

Setting $i = 0$ and using $\tau_0 = 0$ yields

$$\begin{aligned}e^{-\tau_1/T_1} &= e^{-\tau_0/T_1} - \frac{1}{N} \\ e^{-\tau_1/T_1} &= 1 - \frac{1}{N} \\ \implies \tau_1 &= -T_1 \ln\left(1 - \frac{1}{N}\right)\end{aligned}$$

Then, by induction

$$\begin{aligned}e^{-\tau_{i+1}/T_1} &= e^{-\tau_i/T_1} - \frac{1}{N} \\ \implies \tau_{i+1} &= -T_1 \ln\left(e^{-\tau_i/T_1} - \frac{1}{N}\right)\end{aligned} \tag{A.3}$$

As it is experimentally impossible to access the true $\hat{M}(0)$, it is necessary to omit the value $\tau = 0$ from the τ-list. The first τ-value, τ_1, should then be ass small as experimentally possible, before computing the rest of the values. As inversion recovery–experiments are performed in order to estimate T_1, an educated guess is needed as an approximate value when inserting to equation A.3.

A.2 Implementation as `R`-code

The above derivation is implemented as `R`-code. Note that in some cases, the last calculated value will yield the logarithm to a negative number. In such case, a smaller number of values or a larger estimate for T_1 can be used. The list is then printed as a .txt-file.

```
1  ######################################################
2  # Script for making time array for T1-measurements
3  # Espen Hagen Blokkdal, e.h.blokkdal@kjemi.uio.no
4  # January 2014
5
6  rm(list=ls(all=TRUE)) # Clear all stored variables
7
8  # tau0 is the first tau-value, N is the number of points
     and T1 is the educated quess for the T1-value. d is
     the number of digits for each tau-value
9
10 t1_est <- function(tau0 = 0.1, N = 50, T1 = 5, dnum = 3){
11
12 # tau0, N and T1 are default values. At least one must be
      specified, values that aren't specified assumes the
     default value (If you don't specify at least one value
     , R will just print the source code)
13
14 tau = rep(NA,N)
15
16 tau[1] = tau0
17
18 for(i in 2:N){
19 tau[i] = round(-T1*log(exp(-tau[i-1]/T1)-1/N), digits =
     dnum)
20 }
21
22 frame <-data.frame(tau)
23
24 write.table(frame, file = "tau_list.txt",
25 row.names = FALSE, col.names = FALSE,
26 quote = FALSE, append = FALSE)
27 }
28
29 # End of script
30
31 ######################################################
```

t1.R

Appendix B

The Establishment of a Steady-State Magnetism

When working with certain compounds, it is experimentally difficult to obtain good data sets due to long spin-lattice relaxation time, T_1. When performing any repetition of experiments in NMR, it is essential to have a repeatable magnetization vector for each experiment, for which one usually waits a time interval, RD, equal to 5 of 3 times T_1 as the recovered normalized magnetization $\hat{M}$ obtained for experimental use then becomes

$$\hat{M} = 1 - e^{-5} \approx 0.99 \qquad \text{or} \qquad \hat{M} = 1 - e^{-3} \approx 0.95$$

If a given sample displays a long T_1, in the order of tens of seconds, this implies RD to be in the order of minutes. In theory this is not a problem, but in practice there are often limitations to hardware or software used for the experiments with restrictions to the allowed *Acquisition Time*, AP, given as the Repetition Delay plus the experimental time. This implies that a long RD will compromise the experimental time, in forms of the number of echoes sampled in a CPMG-experiment, the length of τ-values in an Inversion Recovery-experiment or any time parameter in any given experimental set-up.

The main section of this appendix deals with the effect of truncating the Repetition Delay in order to establish a steady-state magnetism and rather work with this than the usual consensus of 5 or 3 times T_1, in order to obtain better data set without compromising the data acquisition.

B.1 The Effect of Shortened Repetition Delay

The primary restriction for the following calculations will be that the system at hand only contains equivalent protons, as multi-spin systems consists of several signal sources that must be separated, implying the need for a full recovery of the magnetization vector.

Given a system with a magnetization that might be decomposed into one contribution along the z-axis, denoted $M^{\parallel}$, and one perpendicular to this, denoted $M^{\perp}$. The magnetization component after n pulses will be denoted $M_n^{\parallel}$ and $M_n^{\perp}$.

Along the z-axis, the recovered magnetism after n pulses is

$$M_{n+1}^{\parallel} = M_0 - (M_0 - M_n^{\parallel})e^{-t/T1} \tag{B.1}$$

If the magnetization vector is left to relaxate during the interval τ between two pulses, the magnetization components decay as

$$M_{n+1}^{\perp} = -M_n^{\perp} e^{-\tau/T_2} \tag{B.2a}$$

$$M_{n+1}^{\parallel} = M_0 - (M_0 + M_n^{\parallel})e^{-\tau/T_1} \tag{B.2b}$$

If the system is then rotated by a $\pi/2$-pulse in the xy-plane, the rotation takes the form

$$\begin{aligned}\mathbf{M}_{n+1}(\tau) &= \mathbb{R}(\pi/2)\mathbf{M}_n(\tau) \\ &= \begin{pmatrix} 1 & 0 & 0 \\ 0 & 0 & 1 \\ 0 & -1 & 0 \end{pmatrix} \begin{pmatrix} 0 \\ -M^{\perp}e^{-\tau/T_2} \\ M_0 - (M_0 + M^{\parallel})e^{-\tau/T_1} \end{pmatrix} \\ &= \begin{pmatrix} 0 \\ M_0 - (M_0 + M^{\parallel})e^{-\tau/T_1} \\ M^{\perp}e^{-\tau/T_2} \end{pmatrix}\end{aligned} \tag{B.3}$$

with $\mathbb{R}(\theta)$ being the rotation matrix. If left to relax during the repetition delay, RD, the two components of $\mathbf{M}$ evolves as

$$M_n^{\perp} = (M_0 - (M_0 + M_n^{\parallel})e^{-\tau/T_1})e^{-\mathrm{RD}/T_2} \tag{B.4a}$$

$$M_n^{\parallel} = M_0 - (M_0 + M_n^{\perp}e^{-\tau/T_2})e^{-\mathrm{RD}/T_1} \tag{B.4b}$$

evolving as

$$M_{n+1}^{\perp} = (M_0 - (M_0 + M_n^{\parallel})e^{-\tau/T_1})e^{-\mathrm{RD}/T_2} \tag{B.5a}$$

$$M_{n+1}^{\parallel} = M_0 - (M_0 + M_n^{\perp}e^{-\tau/T_2})e^{-\mathrm{RD}/T_1} \tag{B.5b}$$

Now define $\zeta = M_{SS}^{\parallel}$ and $\eta = M_{SS}^{\perp}$ as the steady-state solutions.

$$\eta = \left(M_0 - (M_0 + \zeta)\, e^{-\tau/T_1}\right) e^{-\mathrm{RD}/T_2} \tag{B.6a}$$

$$\zeta = M_0 - \left(M_0 + \eta e^{-\tau/T_2}\right) e^{-\mathrm{RD}/T_1} \tag{B.6b}$$

Which rearranges as

$$\eta = M_0 e^{-\mathrm{RD}/T_2} - M_0 e^{-\tau/T_1 - \mathrm{RD}/T_2} - \zeta e^{-\tau/T_1 - \mathrm{RD}/T_2} \tag{B.7a}$$

$$\zeta = M_0 - M_0 e^{-\mathrm{RD}/T_1} - \eta e^{-\tau/T_2 - \mathrm{RD}/T_1} \tag{B.7b}$$

Inserting η to ζ, the latter expression becomes

$$\begin{aligned}\zeta = M_0 - M_0 e^{-\mathrm{RD}/T_1} - \big(&M_0 e^{-\mathrm{RD}/T_2} \\ &- M_0 e^{-\tau/T_1 - \mathrm{RD}/T_2} - \zeta e^{-\tau/T_1 - \mathrm{RD}/T_2}\big) e^{-\tau/T_2 - \mathrm{RD}/T_1}\end{aligned} \tag{B.8}$$

and the normalized ζ might be retained as

$$\hat{\zeta} = \frac{\zeta}{M_0} = \frac{1 - e^{-\mathrm{RD}/T_1} - e^{-t_{\mathrm{tot}}/T_2 - \mathrm{RD}/T_1} + e^{-t_{\mathrm{tot}}/T_1 - t_{\mathrm{tot}}/T_2}}{1 - e^{-t_{\mathrm{tot}}/T_1 - t_{\mathrm{tot}}/T_2}} \tag{B.9}$$

with $t_{\mathrm{tot}} = \mathrm{RD} + \tau$.

This expression allows for investigating the effect of varying RD on a steady-state magnetization. For fixed values of T_1 and T_2 and varying RD, the expression demonstrates that in the steady-state situation, a prolonged RD yields a larger magnetization vector, but no other effect.

For this thesis, this allows for measurements on benzene. Benzene has a T_1 in order of ten seconds, which implies that only a few echoes may be sampled due to instrumental limitations. When decreasing RD so that RD $= T_1$, ≈ 70 % of the magnetism is recovered, while the number of echoes can be doubled or tripled, improving the signal-to-noise ratio, in addition to give a better description of the relaxation curves.

If eqs. B.4a and B.4b are solved as difference equations, it can be established how many pulses are required before establishing a steady state magnetism as described above. The results are given in fig. B.1. It can be seen from this figure that a steady-state magnetism is established after 3 pulses when $T_1 = T_2 = 10$ s. As a comparison, it is also shown that for $T_1 = T_2 = 5$ s, the steady-state magnetism is established after just a single pulse, whereas for systems with $T_1 = T_2 = 20$ s, a total of 6 or 7 pulses are required. The simplification that $T_1 = T_2$ has been used as they usually are of similar magnitude and can be justified for most simple liquids.

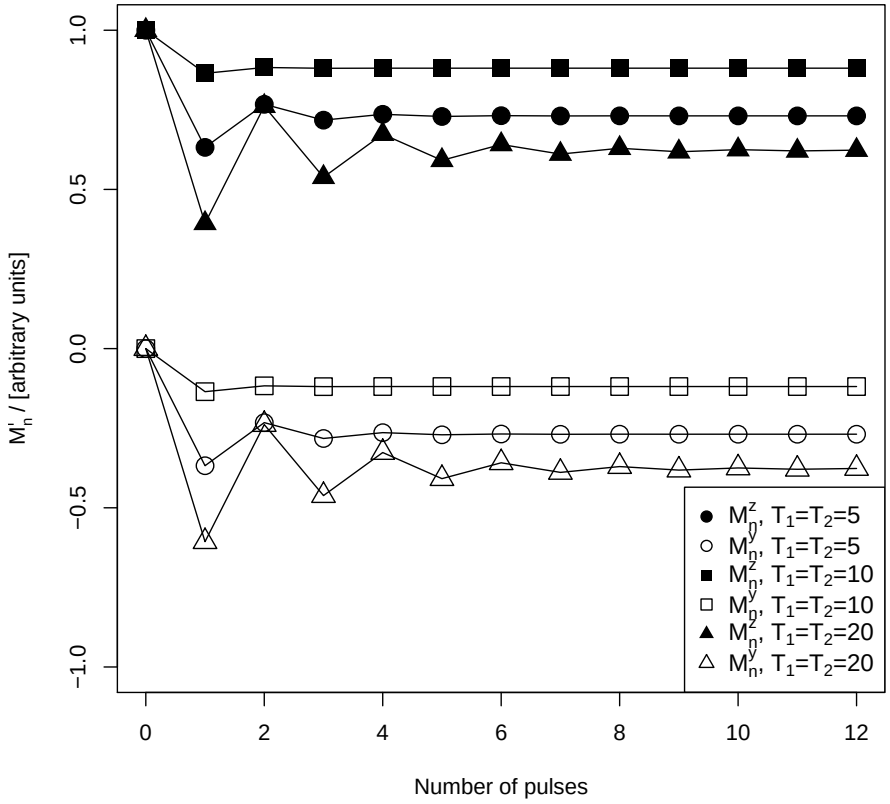

Figure B.1: The effect of consecutive pulses for establishing a steady-state magnetism. The y-axis is given as the n-th components of the magnetization. The first point plotted is the starting magnetism before any pulse has been applied.

Appendix C

Non-Linear Regression Algorithm using R's nls-package

Section C.1 provides a review of the homemade script for analyzing data from CPMG-experiments written in R and using it's nls()-function in addition to the source code. An implementation is given in section C.2 The general algorithm is reviewed in [50]. The convergence properties of the GNA are reviewed in detail in [51, 52].

C.1 R -script for Estimating T_2^*

The step-by-step version of the script t2analyse.R may be given as

1. Remove any previously stored variables.
2. Take the name of the data-file that is to be analyzed as input. The data files might be any form of raw text files.
3. The given file is read and the data stored in arrays.
4. Introducing start-guesses for the various parameters in the model.
5. A dataframe, [34], is constructed from the arrays created earlier.
6. The model is fitted to the data frame, using the start guesses made earlier.
7. The script then produces a plot of the raw data and model and a residual plot. These plot are only saved locally.
8. Finally, the script ends by returning the estimated parameters.

```
# R-script for analysis of T2 measurements by CPMG-NMR
# Espen H. Blokkdal
# e.h.blokkdal@kjemi.uio.no
# Fall 2013, Blindern, Oslo, Norway

rm(list=ls(all=TRUE))

t2analyse <- function(filename, n=1){

#####################################

# Arranging data and declearing variables
SKIP = 0
input <- read.table(filename, header = FALSE, skip = SKIP)
# reading input file and storing it as input

S = 1E0 # Scaling of time parameters, proved unnecessary

t = input[,1] # picking the tau-values
I = sqrt(input[,2]**2 + input[,3]**2) # picking the intensities
tau = t*S  #

# Renaming before fitting
Upsilon = I #(I-I[length(I)])/(max(I)-I[length(I)]) # Removing off-set and scaling by intensity

# guess-values:
T2_guess = 0.4*S # milliseconds
M0_guess = Upsilon[1]
eps_guess = 1


#print("section 2 finished")
#####################################

# Declaring input and model for NLS-fitting for different n, and

frame <- data.frame(x = tau, y = Upsilon)

```

```
39 # non-linear square fit. For further documentation, see
      http://stat.ethz.ch/R-maupsilonal/R-patched/library/
      stats/html/nls.html or Nonlinear Regression with R by
      Ritz and Stribig, Springer, 2008
40
41 fit <- nls(
42 Upsilon~M0*exp(-tau/T2) + eps,
43 data = frame,
44 start = list(M0 = M0_guess, T2 = T2_guess, eps = eps_
      guess))
45 fit.res <- resid(fit)
46
47 #print("section 3 finished")
48 ######################################
49
50 Upsilon_fit = fitted(fit)
51
52 regtab = summary(fit)$coef
53
54 # Generating plot grid based on minimum and maximum
      values
55 par(mfrow=c(2,1))
56 minU = min(Upsilon)
57 maxU = max(Upsilon)
58 mint = min(tau)
59 maxt = max(tau)
60 U = c(0.9*minU, 1.1*maxU)
61 T = c(0.9*mint, 1.1*maxt)
62
63 # plotting
64 plot(T, U, type="n",
65 xlab = "t / [s]",
66 ylab = expression(paste(Upsilon, "(t)/", Upsilon, (0))),
67 main = filename)
68 #sub = "(Number of expontials = 1)"
69 points(tau, Upsilon, col = "black")
70 lines(tau, Upsilon_fit, col = "red", lw = 1.75)
71
72 # Adding legend
73 legend(
74 "topright", legend = c("Data point","exponential \n
      regression"),
```

```
 col = c("black","red"), lty = c(NA,1), lwd = c(NA,2),
    pch = c(1, NA)
)

Rs = 5 # Skalering av residualaksen
R = Rs*c(-max(fit.res), max(fit.res))

plot(xlim = T, ylim = R, type = "l", tau, fit.res, pch =
   1, cex = 1,
ylab="Residual magnitude", xlab="t / [s]",
main="Residual plot")
abline(0, 0, col = "red", lwd = 2)

# Adding legend to residual plot
legend(
"topright", legend = c("Residual", "Zero-line"),
 col = c("black", "red"), lty = c(NA,1), lwd = c(NA,2),
    pch = c(1,NA)
)

#print(regtab)

#M0data <- regtab[1,]
#return(M0data)

T2data <- regtab[2,]/S
return(T2data)
#print("section 4 finished")

}

#
```

t2analyse.R

C.2 Further Implementation to Estimate T_2 and G_1^2

1. The previous script must be loaded to `R` as it is implemented in this algorithm.

2. The name of all data files and parameter files must be entered, along with a list of names for saving the .pdf-files made by the script reviewed in the previous section. This script will later save these .pdf-files globally.

3. A series of various arrays containing only not-a-number-values are created to store temporal values.

4. The τ-values are stored in the list `tau`.

5. The script `t2analyse.R` is run once for each data file and extracts the estimated T_2^* and the estimated M_0.

6. The standard deviation for each set of τ is computed.

7. A plot of the estimated $R_2^* \equiv 1/T_2^*$ against τ^2 is then produced, and weighted linear regression is added together with the measurements and computed standard deviations.

8. The data obtained from regression is saved to a .txt-file.

9. A plot of the estimated M_0 vs. τ is made.

Appendix D

A Generalization of the Hahn Echo and CPMG-signal

D.1 Derivation of the Generalized CPMG-signal

Starting with the normalized CPMG echo intensity in the rotating frame of reference

$$\hat{M}(t) = \exp\left(-\frac{t}{T_2} - \frac{t}{3}D\left(\gamma\tau\frac{\partial B}{\partial z}\right)^2\right) \tag{D.1}$$

with z as the direction along the NMR tube and assuming a polynomial form of B that may be approximated by its second-order Taylor expansion around $z = 0$ as

$$\begin{aligned} B(z) &= \sum_{n=0}^{\infty} \frac{1}{n!} \left.\frac{\partial^n B}{\partial z^n}\right|_{z=0} z^n \\ &\approx B(0) + \left.\frac{\partial B}{\partial z}\right|_{z=0} z + \frac{1}{2} \left.\frac{\partial^2 B}{\partial z}\right|_{z=0} z^2 \\ &\equiv B_0 + G_1 z + G_2 z^2 \end{aligned} \tag{D.2}$$

where the z-axis is taken to be parallel to $\mathbf{B} = B\mathbf{k}$ for a sample with length L. The Taylor expansion is truncated after the second-order term.

The form of eq. D.2 might be rewritten in terms of the Larmour frequency, using

$$\omega = -\gamma B \tag{D.3}$$

so that

$$\omega(z) = -\gamma G(z) = -\gamma\left(G_0 + G_1 z + G_2 z^2\right) = \omega_0 + \omega_1 z + \omega_2 z^2 \tag{D.4}$$

and insertion of eq. D.4 to eq. D.1 yields

$$\begin{aligned}\hat{M}(z,t) &= \exp\left(\frac{-t}{T_2}\right)\exp\left(\frac{-t}{3}D\left(\tau\frac{\partial\omega(z)}{\partial z}\right)^2\right)\\ &= \exp\left(\frac{-t}{T_2}\right)\exp\left(\frac{-t}{3}D\left(\tau(\omega_1+2\omega_2 z)\right)^2\right)\end{aligned} \tag{D.5}$$

As eq. D.5 is dependent on z and eq. D.1 is not, the retrieved signal, that is eq. D.1, must be the sample average. This implies that

$$\begin{aligned}\hat{M}(t) &= \left\langle \hat{M}(z,t)\right\rangle = L^{-1}\int_0^L \hat{M}(z,t)\,\mathrm{d}z\\ &= L^{-1}\exp\left(\frac{-t}{T_2}\right)\int_0^L \exp\left(\frac{-t}{3}D\tau^2\left(\omega_1+2\omega_2 z\right)^2\right)\,\mathrm{d}z\end{aligned} \tag{D.6}$$

and by rewriting $\alpha^2 = \frac{D\tau^2 t}{3}$ and substituting $\zeta = \alpha\omega_1 + 2\alpha\omega_2 z$ the equation now reads:

$$\begin{aligned}\hat{M}(t) &= L^{-1}\exp\left(\frac{-t}{T_2}\right)\int_0^L \exp\left(-\zeta^2\right)\,\mathrm{d}z\\ &= \frac{\exp\left(\frac{-t}{T_2}\right)}{2L\omega_2\alpha}\int_{\alpha\omega_1}^{\alpha\omega_1+2\alpha\omega_2 L}\exp\left(-\zeta^2\right)\,\mathrm{d}\zeta\end{aligned} \tag{D.7}$$

as $\mathrm{d}z = \frac{\mathrm{d}\zeta}{2\omega_2\alpha}$.

The integral above is similar to

$$\int_0^z \exp(-t^2)\,\mathrm{d}t = \frac{\sqrt{\pi}}{2}\mathrm{erf}(z)$$

where $\mathrm{erf}(z)$ is the error function[53].

This gives that eq. D.7 acn be solved as

$$\begin{aligned}\hat{M}(t) &= \frac{\exp\left(\frac{-t}{T_2}\right)}{2L\omega_2\alpha}\int_{\alpha\omega_1}^{\alpha\omega_1+2\alpha\omega_2 L}\exp\left(-\zeta^2\right)\,\mathrm{d}\zeta\\ &= \frac{\exp\left(\frac{-t}{T_2}\right)}{2L\omega_2\alpha}\frac{\sqrt{\pi}}{2}\left(\mathrm{erf}\left(\alpha\omega_1+2\alpha\omega_2 L\right)-\mathrm{erf}\left(\alpha\omega_1\right)\right)\\ &= \frac{\sqrt{3\pi}}{4L\omega_2\tau\sqrt{Dt}}\exp\left(\frac{-t}{T_2}\right)\left(\mathrm{erf}\left(\alpha\omega_1+2\alpha\omega_2 L\right)-\mathrm{erf}\left(\alpha\omega_1\right)\right)\end{aligned} \tag{D.8}$$

where the erf(z)-function might be approximated by its Taylor expansion around $z = 0$ as

$$\mathrm{erf}(z) = \frac{2}{\sqrt{\pi}} \sum_{n=0}^{\infty} \frac{(-1)^n}{n!(2n+1)} \, z^{2n+1}\Big|_{z=0}$$

so that eq. D.8 might be expanded around $\alpha = 0$ as

$$\begin{aligned}
\hat{M}(t) &= \frac{2}{\sqrt{\pi}} \frac{\sqrt{3\pi}}{4L\omega_2\tau\sqrt{Dt}} \exp\left(\frac{-t}{T_2}\right) \left(\sum_{n=0}^{\infty} \frac{(-1)^n(\alpha\omega_1 + 2\alpha\omega_2 L)^{2n+1}}{n!(2n+1)} - \sum_{n=0}^{\infty} \frac{(-1)^n(\alpha\omega_1)^{2n+1}}{n!(2n+1)} \right) \\
&\approx \frac{\sqrt{3}}{2L\omega_2\tau\sqrt{Dt}} \exp\left(\frac{-t}{T_2}\right) \left((\alpha\omega_1 + 2\alpha\omega_2 L) - \frac{(\alpha\omega_1 + 2\alpha\omega_2 L)^3}{3} - \alpha\omega_1 + \frac{(\alpha\omega_1)^3}{3} \right) \\
&= \exp\left(\frac{-t}{T_2}\right) \left(1 - t\frac{D\tau^2}{18L\omega_2} \left((\omega_1 + 2\omega_2 L)^3 - \omega_1^3 \right) \right) \\
&= \exp\left(\frac{-t}{T_2}\right) \left(1 - t\frac{D\tau^2}{9} \left(3\omega_1^2 + 6L\omega_2\omega_1 + 4L^2\omega_2^2 \right) \right) \qquad \text{(D.9)}
\end{aligned}$$

when substituting $\alpha^2 = \frac{D\tau^2 t}{3}$. As the error function has been expanded in α to second order, the expansion is to first order in t.

Finally, eq. D.9 might be recognized as the first-order Taylor expansion of e^{-t}, as

$$\exp(-t) = \sum_{n=0}^{\infty} \frac{(-1)^n}{n!}\bigg|_{t=0} t^n \approx 1 - t$$

Under this assumption, the closed form of the signal becomes

$$\begin{aligned}
\hat{M}(t) &= \exp\left(-\frac{t}{T_2} - t\frac{D\tau^2}{9} \left(3\omega_1^2 + 6L\omega_2\omega_1 + 4L^2\omega_2^2 \right) \right) \\
&= \exp\left(-\frac{t}{T_2} - t\frac{D\gamma^2\tau^2}{9} \left(3G_1^2 + 6LG_2G_1 + 4L^2G_2^2 \right) \right) \qquad \text{(D.10)}
\end{aligned}$$

and we see that in the case where $G_2 = 0$, the form of eq. D.1 is retained.

The signal for the Hahn echo experiment is then obtained by substituting $t = 2N\tau$ with $N = 1$ in eq. D.10:

$$\hat{M}(\tau) = \exp\left(-\frac{2\tau}{T_2} - \frac{2D\gamma^2\tau^3}{9} \left(3G_1^2 + 6LG_2G_1 + 4L^2G_2^2 \right) \right) \qquad \text{(D.11)}$$

Bibliography

[1] Weast, R. C. *Handbook of Chemistry and Physics* (CRC, 1970), 51st edn.

[2] Levitt, M. H. *Spin Dynamics - Basics of Nuclear Magnetic Resonance* (John Wiley & Sons Ltd, 2008), 2nd edn.

[3] Hahn, E. L. Spin echoes. *Phys. Rew.* **80**, 580–594 (1950).

[4] Carr, H. Y. & Purcell, E. M. Effects of diffusion on free precession in nuclear magnetic resonance experiments. *Phys. Rew.* **94**, 630–638 (1954).

[5] Meiboom, S. & Gill, D. Modified spin-echo method for measuring nuclear relaxation times. *Rev. Sci. Instrum.* **29**, 688–691 (1958).

[6] Packer, K. The effects of diffusion through locally inhomogeneous magnetic fields on transverse nuclear spin relaxation in heterogeneous systems. proton transverse relaxation in striated muscle tissue. *J. Magn. Res.* **9**, 438–443 (1973).

[7] Hürlimann, M. D. & Griffin, D. D. Spin dynamics of Carr-Purcell-Meiboom-Gill-like sequences in grossly inhomogeneous B_0 and B_1 fields and application to NMR well logging. *J. Magn. Res.* **143**, 120–135 (2000).

[8] Bloch, F. Nuclear induction. *Phys. Rew.* **70**, 460–474 (1946).

[9] Torrey, H. C. Bloch equation with diffusion terms. *Phys. Rew.* **104**, 563–565 (1956).

[10] Doussal, P. L. & Sen, P. N. Decay of nuclear magnetization by diffusion in a parabolic magnetic field: an exactly solvable model. *Phys. Rew. B* **46**, 3465–3485 (1992).

[11] Ulrich, K., Centeno, S. A., Arslanoglu, J. & Federico, E. D. Absorption and diffusion measurements of water in acrylic paint films by single-sided NMR. *Prog. Org. Coat.* **71**, 283–289 (2011).

[12] Donkers, P. A. J., Huinink, H. P., Erich, S. J. F., Reuvers, N. J. W. & Adan, O. C. G. Water permeability of pigmented waterborne coatings. *Prog. Org. Coat.* **76**, 60–69 (2013).

[13] Christensen, M. *Developing new consolidants for archeological wood.* Ph.D. thesis, University of Oslo (2004).

[14] Seland, J. G. & Aaserud, S. Characterization of apple juice by use of diffusion-ordered NMR spectroscopy. The 13$^{\text{th}}$ National MR Meeting (2014).

[15] Vlaardingerbroek, M. T. & den Boer, J. A. *Magnetic Resonance Imaging - Theory and Practice* (Springer, 2003), 3rd edn.

[16] Levine, I. *Physical Chemistry* (McGraw-Hill, 2008), 6th edn.

[17] Price, W. S. *NMR Studies of Translational Motion* (Cambridge University Press, 2009), 1st edn.

[18] Tyrrell, H. J. & Harris, K. R. *Diffusion in Liquids* (Butterworths, 1984), 1st edn.

[19] Hansen, E. W. & Blokkdal, E. H. Self-diffusion coefficient of bulk fluids confined in an inhomogeneous magnetic field (characterized by a second order polynomial with respect to the field direction) as probed by CPMG NMR – influence on sample geometry, sample length and sample position. *In preparation* .

[20] Lillestøl, E., Hunderi, O. & Lien, J. R. *Generell fysikk for universiteter og høgskoler, bind 2* (Universitetsforlaget, 2006), 1st edn.

[21] Fick, A. Ueber diffusion. *Ann. Phys. Chem* **170**, 59–86 (1855).

[22] Brown, R. A brief account of microscopical observations made in the months of June, July and August, 1827, on the particles contained in the pollen of plants; and on the general existence of active molecules in organic and inorganic bodies. *Phil. Mag.* **4**, 161–173 (1828).

[23] Tritton, D. J. *Physical Fluid Dynamics* (Oxford University Press, 1988), 2nd edn.

[24] Riley, K. F., Hobson, M. P. & Bence, S. J. *Mathematical Methods for Physics and Engineering* (Cambridge University Press, 2012), 3rd edn.

[25] Holz, M., Heil, S. R. & Sacco, A. Temperature-dependent self-diffusion coefficients of water and six selected molecular liquids for calibration in accurate ^{1}H NMR PFG measurements. *Phys. Chem. Chem. Phys.* 4040–4742 (2000).

[26] Bergman, T. L., Lavine, A. S., Incropera, F. P. & Dewitt, D. P. *Fundamentals of Heat and Mass Transfer* (John Wiley & Sons, 2011), 7th edn.

[27] Cross, M. & Greenside, H. *Pattern formation and dynamics in nonequilibrium systems* (Cambridge University Press, 2009), 1st edn.

[28] Nicolis, G. *Introduction to Nonlinear Science* (Cambridge University Press, 1995), 1st edn.

[29] Donaldson, I. G. Free convection in a vertical tube with a linear wall temperature gradient. *Aust. J. Phys.* **14**, 529–539 (1961).

[30] Bloembergen, N., Purcell, E. M. & Pound, R. V. Relaxation effects in nuclear magnetic resonance absorption. *Phys. Rew.* **73**, 679–715 (1947).

[31] Friebolin, H. *Basic One- and Two-Dimensional NMR Spectroscopy* (Wiley-VCH, 2013), 5th edn.

[32] Schlicter, C. P. *Principles of Magnetic Resonance* (Springer-Verlag, 1978), 2nd, reviced and expanded edn.

[33] Vold, R. L. & Vold, R. R. Nuclear magnetic relaxation in coupled spin systems. *Prog. Nucl. Magn. Reson. Spectrosc.* **12**, 79–133 (1978).

[34] Crawley, M. J. *The `R` Book* (John Wiley & Sons, 2013), 2nd edn.

[35] Ritz, C. & Streibig, J. C. *Nonlinear Regression with `R`* (Springer, 2008), 1st edn.

[36] The Merck Index* Online. `https://www.rsc.org/Merck-Index/`. Accessed: 22-06-2014.

[37] Bendiksen, B. Benzenmobilitet i MOF UiO-67: lavfelt-^{1}H-NMR-målinger, og simuleringer (2014).

[38] Yoshida, K., Matubayasi, N. & Nakahara, M. Self-diffusion coefficients for water and organic solvents at high temperature along the coexistence curve. *J. Chem. Phys.* (2008).

[39] Computer Hope. `http://www.computerhope.com/jargon/r/refrrate.htm`. Accessed: 23-06-2014.

[40] Huber, P. J. & Ronchetti, E. M. *Robust Statistics* (John Wiley & Sons, 2009), 2nd edn.

[41] Hirasaki, G. J., Lo, S.-W. & Zhang, Y. NMR properties of petroleum reservoir fluids. 679–715 (6th International Conference on Magnetic Resonance in Porous Media, Ulm, Germany, September 8-12, 2002, 2002).

[42] Gaylord Chemical Corporation. Dimethyl sulfoxide (DMSO) physical properties. Bulletin nr. 101 (2005).

[43] Tasioulamargari, M. & Demetropoulos, I. N. Viscosities of dilute solutions of the triglycerides triolein, trilinolein, tristearin, tripalmitin, and trimyristin in benzene and p-xylene. *J. Chem. Eng. Data* **37**, 77–79 (1992).

[44] Krestov, G. A. Polythermische untersuchung der dichte und viskosität von tetra(tert-butyl)tetraphenylporforin. *Viniti* .

[45] Ravikovich, S. D. Viskosität von binären flüssigen mischungen und lösungen. *Zh. Fiz. Khim.* **24**, 524–528 (1950).

[46] G. Tardajos, E. A. & Peña, M. D. Isobaric thermal expansion coefficient of benzene + n-decane, and + n-tetradecane mixtures at various temperatures. *Fluid Phase Equilibr.* **20**, 87–92 (1985).

[47] Nath, J. & Dixit, A. P. Ultrasonic velocities in, and adiabatic compatibilities and excess volumes for, binary liquid mixtures of acetone with tetrachloroethylene, trichloroethylene, methylene chloride, 1,2-dichloroethane, and cyclohexane. *J. Chem. Eng. Data* **29**, 313–316 (1984).

[48] Dymond, J. H. & Young, K. J. Transport properties of nonelectrolyte liquid mixtures - I. viscosity coefficients for n-alkane mixtures at saturation pressure from 283 to 378 K. *Int. J. Thermophys* **1**, 331–344 (1980).

[49] Verdier, S. & Andersen, S. I. Determination of isobaric thermal expansivity of organic compounds from 0.1 to 30 MPa at 30 °C with an isothermal pressure scanning microcalorimeter. *J. Chem. Eng. Data* **48**, 892–897 (2003).

[50] Bates, D. M. & Watts, D. G. *Nonlinear Regression Analysis and its Applications* (John Wiley & Sons, 1988), 1st edn.

[51] Dennis, J. E. & Schnabel, R. B. *Numerical Methods for Unconstrained Optimization and Nonlinear Equations* (Prentice-Hall: Englewood Cliffs, NJ, 1983), 1st edn.

[52] Lootsma, F. A. *Numerical Methods for Nonlinear Optimization* (Academic Press; London, 1972), 1st edn.

[53] Olver, F. W. J., Lozier, D. W., Boisvert, R. F. & Clark, C. W. *NIST Handbook of Mathematical Functions* (Cambridge University Press, 2010).